



"El saber de mis hijos
hará mi grandeza"

UNIVERSIDAD DE SONORA

DIVISIÓN DE CIENCIAS EXACTAS Y NATURALES

Programa de Posgrado en Matemáticas

A Mathematical Model of Dengue Dynamics Based on
Epidemiological Data.

T E S I S

Que para obtener el grado académico de:

Maestro en Ciencias
(Matemáticas)

Presenta:

Claudia Elizabeth Hawks Gutiérrez.

Director de Tesis: Dr. Jorge X. Velasco Hernández
Dr. Daniel Olmos Liceaga

Hermosillo, Sonora, México, Junio de 2013

Universidad de Sonora

Repositorio Institucional UNISON



**"El saber de mis hijos
hará mi grandeza"**



Excepto si se señala otra cosa, la licencia del ítem se describe como openAccess

SINODALES

Dr. Fernando Verduzco González
Universidad de Sonora

Dr. Martín Gildardo García Alvarado
Universidad de Sonora

Dr. Jorge X. Velasco Hernández
Instituto Mexicano del Petróleo

Dr. Daniel Olmos Liceaga
Universidad de Sonora

Contents

1	Two strains model	3
1.1	The Feng-Velasco Model	3
1.2	A New Model	5
1.3	Parameters of the Model	8
2	Basic Reproductive Number	9
2.1	Introduction	9
2.2	Equilibrium Points	9
2.3	Calculation of the Basic Reproductive Number	12
2.3.1	First Calculation	13
2.3.2	Second Calculation	17
2.4	Some Conclusions on the Basic Reproductive Number	20
3	Numerical Studies	23
3.1	Bifurcation Analysis for β_i	23
3.1.1	Analysis of the bifurcation value for β_i in terms of R_0	25
3.2	Regions	26
3.2.1	Parameters	26
3.2.2	Regions	27
3.2.3	Initial Conditions	28
3.3	Simulations	28
3.3.1	Region I - Autonomous Case	29
3.3.2	Region I - Seasonality Case	33
3.3.3	Region II - Autonomous Case	35
3.3.4	Region II - Seasonality Case	37
3.3.5	Region III - Autonomous Case	39
3.3.6	Region III - Seasonality Case	41
3.3.7	Region IV - Autonomous Case	45
3.3.8	Region IV - Seasonality Case	46
3.3.9	Observations	47

4	Wavelets	49
4.1	An Introduction to Wavelets	49
4.2	Analysis of the Model Using Wavelets	55
4.3	Comparison with Four Mexican States data	56
4.4	Comparison with Cuernavaca Data	63
4.5	Comparison with Google Trends Data	67
4.6	Conclusions	70
5	Conclusions	71
A	Operator $\phi(K)$	73

Introduction

Dengue is an infectious tropical disease caused by the dengue virus. It is also known as breakbone fever due to the sensation the disease produces. The symptoms include fever, headache, muscle and joint pains, and a skin rash that is similar to measles which last from three to seven days. In very few cases the disease leads to a life-threatening type of dengue called dengue hemorrhagic fever, which causes internal bleeding. Also, the dengue shock syndrome is another manifestation of the dengue disease where low blood pressure occurs which places the patient in a danger which can lead to death [53].

Dengue is transmitted by two species of mosquitoes, *Aedes aegypti* type or *Aedes albopictus* type. Mosquitoes grow in recipients which gather clean water from rain or dew. There are four different strains of dengue: DEN-1, DEN-2, DEN-3, and DEN-4. Once a patient has been infected with one of these strains, he or she acquires lifetime immunity to that strain but only short-term immunity to others. This subsequent infections with different strains increase the risk of severe complications [53].

Dengue disease affects mainly tropical and subtropical areas like Africa, north of Australia, and America; although lately Europe and North America have reported some cases. So far there no vaccine for dengue has been applied, but several prevention measures have been taken to reduce the effective contact of infected mosquitoes with humans and the elimination of the mosquitoes habitats [53].

Many studies have been made in order to get a better comprehension of Dengue dynamics, for example, in Mosquera studies [36] they present the dynamics of transmission of one dengue virus serotype by means of an aquatic predator. Mosquera studies the dynamics of Dengue considering host population with SIR model to describe their dynamic and vector populations using SI models to describe its dynamic. Another example of the studies made on Dengue disease is the model of Feng-Velasco[17] which we have taken as the starting point for this work and will be explained lately. In Derouich [10] they consider a SIR model to study a 2-strain dynamic where the latent stage is not incorporated. Also, in the studies of Favier [16] on Dengue modelling where they analyze it at different scales (as town, region, continent) and discusses the work yet to be done in this area. Indeed there is a lot to be done since this topic is very complex and there is nothing conclusive yet.

For Dengue disease it is known there are four strains of Dengue circulating in the world, although in Mexico it is known there are two, that is why the model we present here considers only two strains of the disease. Some models have already

been done of this disease, as we mentioned before, but the purpose we are following is to get a better comprehension of the disease dynamics and we decided to start this study taking only two strains in consideration for simplicity and we leave the three and fourth strains models to be studied in a latest case.

The purpose of this thesis is to get a better comprehension of the dengue dynamics with the intention of developing a tool which would allow the study of the evolution of the disease in the future. We present a model which considers two strains to study the dynamics of dengue in Mexico which includes a latency stage. We want to understand the dynamics of this new model and we want to know if it can be applied in the analysis of a real situation in a Mexican community where dengue already exist.

We will study the proposed model by making use of mathematical and computational resources. By analyzing the model for equilibrium points and the parameters involved in the search of bifurcations we pretend to study the space of parameters and to see if we can reduce it. With algebra methods we will calculate the basic reproductive number which is determinant to understand the impact of the disease in a population. Also, we will make use of numerical analysis to obtain the solutions of the model and to run simulations. And finally, we will implement wavelets to see if the model fits real data and can be used to study a real situation.

What distinguishes the model we will introduce here is that it takes into account the dynamics among mosquitoes as well as the dynamics among host with a more complex model which considers a latency stage before the host becomes infected. Also we want to see the importance of considering seasonal periodicity in the model, thus we will simulate and compare the results of the model with and without annual forced periodicity.

This study has the following order: In Chapter 1 we introduce the new model and describe the parameters. In Chapter 2, we present the calculations for the Basic Reproductive Number and we made an analysis of the more significant parameters involved in the expression we obtained of R_0 . In Chapter 3 we show some results and simulations we obtained from the model. Finally, in Chapter 4 we make use of wavelets as a tool to compare the data we got from the simulations of the model with real data from Mexican databases.

Chapter 1

Two strains model

This thesis is limited to the situation where only two strains co-circulate in a human population. We will present first a model that has been taken as starting point to this text and which was developed by Feng and Velasco [17] and involves two strains of the Dengue disease. The stages are Susceptible, Infected (first by one strain and then by the other), Temporally immune (after the first infection) and at last Recovered. Later, we will introduce a new model, and we will refer to it as "the model", where we describe the Dynamics of Dengue considering a new stage named Latency stage, where we will have all humans that are infected with the disease but they do not show any symptoms (and probably never will). Also in the model we will take into consideration the dynamics of mosquitoes as they interact with humans.

1.1 The Feng-Velasco Model

The present model was developed and studied by Feng and Velasco [17].

The letter S represents the susceptible individuals which are exposed to infection by any strain, λ is the recruitment rate and μ the mortality rate by natural causes other than the disease.

Infection in humans is acquired through the biting of infected mosquitoes with either of the two strains (and mosquitoes get infected when biting an infected human by any strain, too). The primary infection produces two types of infected human hosts identified by the strain that was transmitted as I_1 and I_2 respectively; infection occurs at rates B_1S and B_2S which are the forces of infection of each strain. The primary infection stage lasts $1/\gamma_i$ days (with $i = 1, 2$).

After they recovered, we assume that individuals become temporarily protected against both strains, so E_1 and E_2 represent individuals with temporal immunity acquired through interaction with strains 1 and 2, respectively. After a time $1/\eta_i$ these individuals lose the immunity to the strain to which they have not yet been contaminated and become susceptible to it. Let T_1 and T_2 represent the susceptible individuals already permanently immune to strain 1 and 2, respectively.

Infection by the other strain in each case can occur but possibly with a lower force of infection $\sigma_i B_i$, $i = 1, 2$, $0 \leq \sigma_i \leq 1$, due to partial cross immunity. Here Y_1 represents a secondary dengue infection due to strain 1; while Y_2 represents a secondary infection due to strain 2. After a time $1/\gamma_i$ individuals become permanently immune to both strains of virus. The equations of this model are:

$$\begin{aligned}
\frac{d}{dt} S &= \lambda - (B_1 + B_2) S - \mu S \\
\frac{d}{dt} I_1 &= B_1 S - (\mu + \gamma_1) I_1 \\
\frac{d}{dt} I_2 &= B_2 S - (\mu + \gamma_2) I_2 \\
\frac{d}{dt} E_1 &= \gamma_1 I_1 - (\mu + \eta_1) E_1 \\
\frac{d}{dt} E_2 &= \gamma_2 I_2 - (\mu + \eta_2) E_2 \\
\frac{d}{dt} T_1 &= \eta_1 E_1 - (\sigma_2 B_2 + \mu) T_1 \\
\frac{d}{dt} T_2 &= \eta_2 E_2 - (\sigma_1 B_1 + \mu) T_2 \\
\frac{d}{dt} Y_1 &= \sigma_1 B_1 T_2 - (\gamma_1 + \mu + m_1) Y_1 \\
\frac{d}{dt} Y_2 &= \sigma_2 B_2 T_1 - (\gamma_2 + \mu + m_2) Y_2 \\
\frac{d}{dt} R &= \gamma_1 Y_1 + \gamma_2 Y_2 - \mu R
\end{aligned} \tag{1.1}$$

Here the total host population is given by the expression

$$N = S + I_1 + I_2 + E_1 + E_2 + T_1 + T_2 + Y_1 + Y_2 + R$$

The following equations for mosquito populations are given to complete the model:

$$\begin{aligned}
\frac{d}{dt} V_0 &= q(t) - (A_1 + A_2) V_0 - \delta V_0 \\
\frac{d}{dt} V_1 &= A_1 V_0 - \delta V_1 \\
\frac{d}{dt} V_2 &= A_2 V_0 - \delta V_2
\end{aligned} \tag{1.2}$$

where $q(t)$ is the rate at which the mosquito population is increasing ($q(t) > 0$ for all values of t), it depends on time due the nature of mosquitoes cycle which depends on climate conditions and the year season among others. A_1 , A_2 represent the force of infection of strain 1 and 2, respectively, among mosquitoes. δ is the rate at which mosquitoes die. The total mosquito population is given by $M = V_0 + V_1 + V_2$.

At this point, there are different hypothesis about the dynamics of mosquitoes and we will discuss two in the following cases.

Case I:

If V_0 represents the susceptible mosquitoes not yet infected, and V_1 and V_2 the number of mosquitoes infected with strain 1 and 2 respectively, then taken

$$B_i = \beta_i V_i / M$$

with $i = 1, 2$, as the force of infection means to assume that it is determined by the proportion of infected mosquitoes among the entire human population.

Define

$$A_i = \alpha_i (I_i + Y_i) / N$$

with $i = 1, 2$, as the force of infection among mosquitoes. It's given by the proportion of infected human host in the entire human population which implies that there's a direct relation among infected humans and infected mosquitoes.

Case II:

If V_0 represents the the susceptible mosquitoes not yet infected, and V_1 and V_2 the number of mosquitoes infected with strain 1 and 2 respectively, then taken $B_i = \beta_i V_i / (c + \omega_h N)$, $i = 1, 2$ leads to conclude that the force of infection in humans depends on the total of infected mosquitoes among a constant c plus a fraction of the total human population.

For this case the force of infection among mosquitoes is given by

$$A_i = \alpha_i (I_i + Y_i) / (c + \omega_i N)$$

and it is shown that again the force of infection among mosquitoes depends complete in the total of infected humans.

1.2 A New Model

Now we will introduce a new model which considers a stage between both susceptible and infected. This is the latency stage where the human host has the infection but is not yet capable of transmission, and perhaps is not even showing any signs or symptoms. We will represent this new stage in the model with the letters C and T .

As before, we will use S to represent the susceptible individuals, with λ as its recruitment rate and mortality rate μ for natural cases other than dengue disease. Infection is acquired through the biting of infected mosquitoes with either of those two strains (denoted by V_1 and V_2); this primary infection produces two types of infected but not infectious human hosts (meaning that they are not contagious) identified by the strain that was transmitted (C_1 and C_2); infection occurs at rates $B_1 S$ and $B_2 S$ which are the forces of infection of each strain. This stage of latency lasts $1/\phi_1$ (or $1/\phi_2$) days.

After this stage the host becomes capable of transmission of the disease to other humans in the infectious stage (I_1 and I_2) which lasts $1/\gamma_i$ days. Then, comes a stage where individuals become temporarily protected against both strains, so E_1 and E_2 represent individuals with temporal immunity (to both strains) acquired through interaction with strains 1 and 2 respectively. After a time $1/\eta_i$ these individuals lose immunity to the strain to which they have not been exposed and become susceptible

to it.

T_1 and T_2 represent the susceptible individuals already permanently immune to strain 1 and 2 respectively. Infection by the other strain in each case can occur but possibly with a lower force of infection $\sigma_i B_i$, with $0 \leq \sigma_i \leq 1$ for $i = 1, 2$, due to partial-cross-immunity.

Here Z_1 represents a secondary dengue infection (in the period of incubation, where the human host is not contagious) due to strain 1; while Z_2 represents a secondary infection to strain 2; this stage lasts $1/\gamma$ days. Then the host becomes contagious for a period of $1/\gamma_i$ during the stage Y_1 or Y_2 , respectively for strains 1 and 2. After this, individuals become permanently immune to both strains of virus in R stage. In the case of mosquitoes, V_0 represents the susceptible vectors. A_1, A_2 represent the forces of infection at which mosquitoes get infected when they get in contact with an infected human.

At the second infection stages Y_i , $i = 1, 2$, the term $m_i Y_i$ appears to represent those cases where the host dies due to the disease, as it is known that Dengue can be fatal in some cases.

The equations for the model are:

$$\begin{aligned}
\frac{d}{dt}S &= \lambda - (B_1 + B_2)S - \mu S \\
\frac{d}{dt}C_1 &= B_1S - (\phi_1 + \mu)C_1 \\
\frac{d}{dt}C_2 &= B_2S - (\phi_2 + \mu)C_2 \\
\frac{d}{dt}I_1 &= \phi_1C_1 - (\mu + \gamma_1)I_1 \\
\frac{d}{dt}I_2 &= \phi_2C_2 - (\mu + \gamma_2)I_2 \\
\frac{d}{dt}E_1 &= \gamma_1I_1 - (\mu + \eta_1)E_1 \\
\frac{d}{dt}E_2 &= \gamma_2I_2 - (\mu + \eta_2)E_2 \\
\frac{d}{dt}T_1 &= \eta_1E_1 - (\sigma_2B_2 + \mu)T_1 \\
\frac{d}{dt}T_2 &= \eta_2E_2 - (\sigma_1B_1 + \mu)T_2 \\
\frac{d}{dt}Z_1 &= \sigma_1B_1T_2 - (\phi_1 + \mu)Z_1 \\
\frac{d}{dt}Z_2 &= \sigma_2B_2T_1 - (\phi_2 + \mu)Z_2 \\
\frac{d}{dt}Y_1 &= \phi_1Z_1 - (\gamma_1 + \mu + m_1)Y_1 \\
\frac{d}{dt}Y_2 &= \phi_2Z_2 - (\gamma_2 + \mu + m_2)Y_2 \\
\frac{d}{dt}R &= \gamma_1Y_1 + \gamma_2Y_2 - \mu R \\
\\
\frac{d}{dt}V_0 &= q(t) - (A_1 + A_2)V_0 - \delta V_0 \\
\frac{d}{dt}V_1 &= A_1V_0 - \delta V_1 \\
\frac{d}{dt}V_2 &= A_2V_0 - \delta V_2
\end{aligned} \tag{1.3}$$

The first fourteen equations describe the dynamic of the disease among humans while the last three describe it among mosquitoes. The total host population is

given by the expression

$$N = S + C_1 + C_2 + I_1 + I_2 + E_1 + E_2 + T_1 + T_2 + Z_1 + Z_2 + Y_1 + Y_2 + R$$

and the total vector population is $M = V_0 + V_1 + V_2$.

With the use of the expression $q(t)$ as the incoming mosquitoes in the equation for susceptible mosquitoes, $\frac{d}{dt}V_0$ defined as:

$$q(t) = q_0 (1 + k \cos(2\pi t/365))$$

we can set $q(t)$ as a constant incoming (taking $k = 0$) or we can force annual periodicity into the model (by taking $k = 1$).

The forces of infection human to mosquito is determined by:

$$A_i = \frac{\alpha_i (I_i + Y_i)}{N} \quad (1.4)$$

$i = 1, 2$, where α_i is the effective contact rate of infected humans with uninfected mosquitoes. The forces of infection mosquito to human is given by the expression

$$B_i = \frac{\beta_i V_i}{M} \quad (1.5)$$

$i = 1, 2$, where β_i is the effective contact rate of infected mosquitoes with susceptible humans.

$A_i, i = 1, 2$ is the force of infection given by the product of the effective contact rate human to mosquito (α_i) with the proportion of infected humans that are in the human population. When a healthy mosquito is in contact with an infected human the probability for it to be contaminated (effective contact) is given by the rate α_i . If $\alpha_i = 1$, the probability for a mosquito to get effectively contaminated will depend entirely in the number of infected humans in the population, that is with the probability of getting in contact with the infected humans in the population .

With B_i we have the same case as with A_i , but in this case it refers to the force of infection related to humans given by the product of the effective contact rate mosquito to human (β_i) with the proportion of infected mosquitoes that are in the mosquito population. When a healthy human gets in contact with an infected mosquito, the probability for it to be infected (effective contact) is given by the rate β_i . β_i is a probability which measures the chances of a human to get infected when in contact with contaminated mosquitoes. If $\beta_i = 1$ the probability for a human to get effectively contaminated will depend completely in its chances to find an infected mosquito.

1.3 Parameters of the Model

Table 1.1: Description of Parameters

Parameter	Description	Chosen Values
$1/\mu$	Life expectance for humans	around 70 years (25550 days)
λ	Incoming human population	0.391389432
$1/\phi_i$	Incubation period	4 to 7 days
$1/\gamma_i$	Duration of disease	7 to 15 days
$1/\delta$	Life expectance of mosquitoes	estimated 14 to 21 days as an adult
$1/\eta_i$	Duration of Crossed immunity	estimated 15 to 180 days
σ_i	Reinfection rate	undetermined**
α_i	Effective contact rate human-mosquito	undetermined*
β_i	Effective contact rate mosquito-human	undetermined*
m_i	Rate of death caused by disease	undetermined**
q	Incoming mosquito population	undetermined**

The table (1.1) gives the description for some of the used parameters. Some of its values can be easily determined due to their definition and others are yet imprecisely unknown due to lack of information on the disease. The values for parameters shown in table (1.1) were taken from Velasco-Feng studies [17]. The values which appear as "undetermined" in table have not yet been estimated. Some of them, like the duration of immunity, can vary from one individual to other.

*In this work, we want to focus in those parameters where can have some influence by the use of prevention actions in the population, like the prevention campaigns in a community. It is possible to reduce the effective contact rates of mosquito to human and human to mosquito (α_i and β_i , respectively, $i = 1, 2$) by taking fumigation, or simply by having mosquito nets in windows, doors or around the bed, etc.

**Since the parameters are too many, and to aboard the study of the model in a simple way, we will set some parameters to have null effect. That is to say, we take σ_i , $i = 1, 2$ to be equal to 1, meaning that the size of the impact of getting the disease for the second time will be exactly the same as it was the first time. Also, parameters m_i , $i = 1, 2$ will be equal to 0, which means that nobody dies by the disease. And parameter $q(t)$ that, as was introduced before, will be a constant number for some simulations and will vary its value periodically for others in order to see which one adjust better to reality.

Chapter 2

Basic Reproductive Number

2.1 Introduction

Defined as a threshold quantity denoted by R_0 that determines whether there is an epidemic or not [2]; this number represents the number of secondary infections caused by a single infective introduced into a wholly susceptible population during his infectious period [4]. An expression for R_0 typically involve products of infection rates and durations of infection [49] R_0 is a threshold parameter for the model, such that if $R_0 < 1$ then the Disease Free Equilibrium is locally asymptotically stable and the disease cannot invade the population (eventually the infection dies out), but if $R_0 > 1$, then the Disease Free Equilibrium is unstable and invasion is possible (there can be an epidemic) [48].

The basic reproduction number is defined [17] as the number of secondary infections that a single infectious individual produces in a population where all host are susceptible. It provides an invasive criterion for the initial spread of the virus in a susceptible population. In order to find this important number for the model we needed to find the eigenvalues of the Next Generation Matrix.

2.2 Equilibrium Points

Consider $\omega = (S, C_1, C_2, I_1, I_2, E_1, E_2, T_1, T_2, Z_1, Z_2, Y_1, Y_2, R, V_0, V_1, V_2)$ as the set bounded by the total host and vector population, that is $0 \leq C_i, I_i, E_i, T_i, Z_i, Y_i, R, V_i$ for $i = 1, 2$, and $0 \leq S \leq N$, $0 \leq V_0 \leq M$.

The equilibrium points of the system (1.3) must satisfy the following:

$$\begin{aligned}
\lambda - (B_1 + B_2)S - \mu S &= 0 \\
B_1S - (\phi_1 + \mu)C_1 &= 0 & B_2S - (\phi_2 + \mu)C_2 &= 0 \\
\phi_1C_1 - (\mu + \gamma_1)I_1 &= 0 & \phi_2C_2 - (\mu + \gamma_2)I_2 &= 0 \\
\gamma_1I_1 - (\mu + \eta_1)E_1 &= 0 & \gamma_2I_2 - (\mu + \eta_2)E_2 &= 0 \\
\eta_1E_1 - (\sigma_2B_2 + \mu)T_1 &= 0 & \eta_2E_2 - (\sigma_1B_1 + \mu)T_2 &= 0 \\
\sigma_1B_1T_2 - (\phi_1 + \mu)Z_1 &= 0 & \sigma_2B_2T_1 - (\phi_2 + \mu)Z_2 &= 0 \\
\phi_1Z_1 - (\gamma_1 + \mu + m_1)Y_1 &= 0 & \phi_2Z_2 - (\gamma_2 + \mu + m_2)Y_2 &= 0 \\
\gamma_1Y_1 + \gamma_2Y_2 - \mu R &= 0 & q(t) - (A_1 + A_2)V_0 - \delta V_0 &= 0 \\
A_1V_0 - \delta V_1 &= 0 & A_2V_0 - \delta V_2 &= 0
\end{aligned} \tag{2.1}$$

Solving this system we obtained the following equilibrium points:

Equilibrium point 1: $(S^1 = \frac{\lambda}{\mu}, 0, 0, 0, 0, 0, 0, 0, 0, 0, 0, 0, 0, 0, 0, 0, V_0^1 = \frac{q}{\delta}, 0, 0)$. This is the disease free equilibrium point.

Equilibrium point 2: $(S^2, C_1^2, 0, I_1^2, 0, E_1^2, 0, T_1^2, 0, 0, 0, 0, 0, 0, 0, V_0^2, V_1^2, 0)$, where only strain 1 is present. We have:

$$\begin{aligned}
S^2 &= \frac{\lambda(\delta(\phi_1 + \mu)(\gamma_1 + \mu) + \phi_1\alpha_1\mu)}{\mu\phi_1(\mu + \beta_1)\alpha_1} \\
C_1^2 &= \frac{-\lambda(\delta(\phi_1 + \mu)(\gamma_1 + \mu) - \alpha_1\beta_1\phi_1)}{\alpha_1\phi_1(\beta_1 + \mu)(\phi_1 + \mu)} \\
I_1^2 &= \frac{-\lambda(\delta(\phi_1 + \mu)(\gamma_1 + \mu) - \alpha_1\beta_1\phi_1)}{\alpha_1(\beta_1 + \mu)(\gamma_1 + \mu)(\phi_1 + \mu)} \\
E_1^2 &= \frac{-\gamma_1\lambda(\delta(\phi_1 + \mu)(\gamma_1 + \mu) - \alpha_1\beta_1\phi_1)}{\alpha_1(\beta_1 + \mu)(\gamma_1 + \mu)(\phi_1 + \mu)(\eta_1 + \mu)} \\
T_1^2 &= \frac{-\eta_1\gamma_1\lambda(\delta(\phi_1 + \mu)(\gamma_1 + \mu) - \alpha_1\beta_1\phi_1)}{\alpha_1\mu(\beta_1 + \mu)(\gamma_1 + \mu)(\phi_1 + \mu)(\eta_1 + \mu)} \\
V_0^2 &= \frac{q(\beta_1 + \mu)(\gamma_1 + \mu)(\phi_1 + \mu)}{\beta_1(\delta(\phi_1 + \mu)(\gamma_1 + \mu) + \phi_1\alpha_1\mu)} \\
V_1^2 &= \frac{-q\mu(\delta(\phi_1 + \mu)(\gamma_1 + \mu) - \alpha_1\beta_1\phi_1)}{\delta\beta_1(\delta(\phi_1 + \mu)(\gamma_1 + \mu) + \phi_1\alpha_1\mu)}
\end{aligned}$$

Equilibrium point 3: $(S^3, C_1^3, 0, I_1^3, 0, E_1^3, 0, T_1^3, 0, Z_1^3, 0, Y_1^3, 0, R^3, V_0^3, V_1^3, 0)$, which is another case where only strain 1 exist. We have:

$$\begin{aligned}
S^3 &= \frac{\sigma_1 \lambda}{\mu (\sigma_1 - 1)} \\
C_1^3 &= \frac{-\lambda}{(\sigma_1 - 1)(\phi + \mu)} \\
I_1^3 &= \frac{-\lambda \phi_1}{(\gamma_1 + \mu)(\phi_1 - \mu)(\sigma_1 - 1)} \\
E_1^3 &= \frac{-\lambda \gamma_1 \phi_1}{(\gamma_1 + \mu)(\phi_1 - \mu)(\sigma_1 - 1)(\eta_1 + \mu)} \\
T_1^3 &= \frac{-\nu_1 \lambda \gamma_1 \phi_1}{\mu (\gamma_1 + \mu)(\phi_1 - \mu)(\sigma_1 - 1)(\eta_1 + \mu)} \\
T_2^3 &= \frac{\lambda (\gamma_1 + \mu + m_1) (\delta (\sigma_1 - 1) (\gamma_1 + \mu) (\phi_1 + \mu) - \alpha_1 \phi_1 (\beta_1 \sigma_1 + \mu))}{\phi_1 \mu (\gamma_1 + \mu) (\sigma_1 - 1) (\delta m_1 - \alpha_1 \beta_1 \sigma_1 - \alpha_1 \mu)} \\
Z_1^3 &= \frac{\lambda (\gamma_1 + \mu + m_1) (\delta (\sigma_1 - 1) (\gamma_1 + \mu) (\phi_1 + \mu) - \alpha_1 \phi_1 (\beta_1 \sigma_1 + \mu))}{\phi_1 (\gamma_1 + \mu) (\gamma_1 + \mu) (\sigma_1 - 1) (\delta m_1 - \alpha_1 \beta_1 \sigma_1 - \alpha_1 \mu)} \\
Y_1^3 &= \frac{\lambda (\delta (\sigma_1 - 1) (\gamma_1 + \mu) (\phi_1 + \mu) - \alpha_1 \phi_1 (\beta_1 \sigma_1 + \mu))}{(\gamma_1 + \mu) (\gamma_1 + \mu) (\sigma_1 - 1) (\delta m_1 - \alpha_1 \beta_1 \sigma_1 - \alpha_1 \mu)} \\
R^3 &= \frac{\gamma_1 \lambda (\delta (\sigma_1 - 1) (\gamma_1 + \mu) (\phi_1 + \mu) - \alpha_1 \phi_1 (\beta_1 \sigma_1 + \mu))}{\mu (\gamma_1 + \mu) (\gamma_1 + \mu) (\sigma_1 - 1) (\delta m_1 - \alpha_1 \beta_1 \sigma_1 - \alpha_1 \mu)} \\
V_0^3 &= \frac{q (\beta_1 \sigma_1 + \mu)}{(\delta \beta_1 \sigma_1)} \\
V_1^3 &= \frac{-q \mu}{\delta \beta_1 \sigma_1}
\end{aligned} \tag{2.2}$$

The Equilibrium Point 1 has always positive valued coordinates and is biologically acceptable. It represents the ideal case where no human and no mosquito are infected. A population where everyone is healthy and susceptible. The Equilibrium Point 1 is the Disease Free Equilibrium Point.

We have to determine the biological feasibility of Equilibrium Point 2. Regarding S^2 we can say that it is always positive, so is always valid. The same will be concluded for V_0^2 .

For C_1^2 , I_1^2 , E_1^2 , T_1^2 and V_1^2 we must analyze in what case their values would be positive and therefore biologically acceptable. We begin the analysis with C_1^2 . If we want C_1^2 to be no negative it must happen that

$$\frac{-\lambda (\delta (\phi_1 + \mu) (\gamma_1 + \mu) - \alpha_1 \beta_1 \phi_1)}{\alpha_1 \phi_1 (\beta_1 + \mu) (\phi_1 + \mu)} \geq 0$$

or, simply

$$-\lambda (\delta (\phi_1 + \mu) (\gamma_1 + \mu) - \alpha_1 \beta_1 \phi_1) \geq 0$$

this happens if and only if

$$\delta (\phi_1 + \mu) (\gamma_1 + \mu) - \alpha_1 \beta_1 \phi_1 \leq 0$$

if only if

$$\frac{\alpha_1 \beta_1 \phi_1}{\delta (\phi_1 + \mu) (\gamma_1 + \mu)} \geq 1$$

We will get to the same restriction when examining I_1^2 , E_1^2 , T_1^2 and V_1^2 . So, the Equilibrium Point 2 is biologically accepted in the case when

$$\frac{\alpha_1 \beta_1 \phi_1}{\delta (\phi_1 + \mu) (\gamma_1 + \mu)} \geq 1$$

This point represents the case where only Strain 1 subsist in the population and Strain 2 has disappeared. The Equilibrium point 2 is where only strain 1 is present.

As for the equilibrium Point 3, V_0^3 is always positive. Regarding S^3 we can say that will never take zero value, but we must restrict it to be positive. So we have

$$\frac{\sigma_1 \lambda}{\mu (\sigma_1 - 1)} > 0$$

which will happen if and only if $\sigma_1 - 1 > 0$, and this will happen if and only if $\sigma_1 > 1$. But from the beginning we had already set $\sigma_1 \leq 1$ (refer to section 1.2). σ_i is the reinfection rate for humans. Therefore, accepting that $\sigma_i > 1$ would imply that if a host had already been infected once, he or she is more exposed to get Dengue for the second time which it is not the case for Dengue disease. So, the Equilibrium Point 3 is not biologically valid and will be rejected for further analysis.

Additionally, an equilibrium point where both strains coexist has been found numerically. However, it was not possible to determine the algebraic expression and therefore is not included in this text. Numerically, six equilibrium points were found for the system. Always the disease free equilibrium point is one of them. Then there are two equilibrium where only one strain survives (either strain 1 or strain 2). The other three equilibrium points correspond to cases where both strains coexist simultaneously but, numerically can be seen, that only one of them is biologically acceptable. We know, then, that there are 4 equilibrium points for this model.

2.3 Calculation of the Basic Reproductive Number

The Basic Reproductive Number is the most important quantity in every epidemiological study of an infectious disease. It help us to determine in what conditions we may have an epidemiological outbreak or not. If $R_0 < 1$, then on average an infected individual produces less than one new infected individual over the course of its infectious period, and the infection cannot grow. Conversely, if $R_0 > 1$, then each infected individual produces, on average, more than one new infection, and the disease can invade the population [48].

R_0 can also be used to foretell the effects of an effort that can be made to control the disease. For example, when trying to reduce the mosquito population we can take a look to the influence this effect may have into the R_0 value and see if it works or not. Also, R_0 has been defined as the average number of secondary infections produced by an infected individual when in contact with a susceptible population [13].

In order to find an expression for R_0 we define a matrix that relates the numbers of newly infected individuals in each of the categories in consecutive generations [13]. This is called the Next Generation Matrix [11] and it is known to have R_0 as its dominant eigenvalue [13]. We present here two different ways of finding an expression for R_0 for the system problem (1.3). Both methods are directly related with the concept of New Generation Matrix.

2.3.1 First Calculation

R_0 is defined as the average number of new cases of an infection caused by one typical infected individual, in a population consisting of susceptibles only. R_0 is mathematically characterized by regarding infection transmission as a demographic process, where producing offspring is not seen as giving birth in the demographic sense, but as causing a new infection through transmission (this is called an "epidemiological birth"). In a natural way this leads to viewing the infection process in terms of consecutive generations of infected individuals, in complete analogy to demographic generations. Subsequent generations growing in size indicate a growing population (i.e. an epidemic), and growth factor per generation indicates the potential for growth. In a natural way this growth factor is then the mathematical characterization of R_0 [13].

In the model 1.3 we have the population divided into a finite number of discrete categories. One can define a matrix that relates the numbers of newly infected individuals in the various categories in consecutive generations. This matrix is called the Next Generation Matrix (NGM) and was introduced by Diekmann et al. [11].

In the model 1.3 we can associate the subpopulation of individuals who are in a particular state at a given time. It is very common to use the same symbol used as a label for a state and to denote the corresponding subpopulation size, either as a fraction or as a number. The dynamics are generated by a system of nonlinear ordinary differential equations (ODE) that describes the change with time for all subpopulation sizes. For the computation of R_0 , we only regard the states that apply to infected individuals [13].

The Next Generation Matrix is defined as the matrix formed by taking the derived matrix of the system of equations (1.3) and decomposing it as $f - v$, where f is the transmission part that describes the production of new infections, and v is the

transition part that describe the changes in the state including the removal by death or the acquisition of immunity [13]. We find the Jacobian of f and we assign it to F , and the Jacobian of v to V . Thus we can calculate R_0 by finding the spectral radius $\rho(FV^{-1})$ [12].

The matrix FV^{-1} is the expected lifetime number of type i individuals produced by an individual of type j [27]. That is why FV^{-1} is called the Next Generation Matrix.

To calculate R_0 we take the infected subsystem from the original ODE of the model 1.3. The infected subsystem are those equations of the ODE system that describe the production of new infections and changes in state among infected individuals. First step is to linearize the infected subsystem of nonlinear ODE around the infection-free steady state [13].

For the system (1.3) we have f , the vector formed by the new infections in states $C1, C2, I1, I2, Z1, Z2, Y1, Y2, V1, V2$:

$$f = (B_1S \quad B_2S \quad 0 \quad 0 \quad \sigma_1B_1T_2 \quad \sigma_2B_2T_1 \quad 0 \quad 0 \quad A_1V_0 \quad A_2V_0)^t \quad (2.3)$$

Thus, we have that F is given by the Jacobian of f :

$$F = \begin{pmatrix} 0 & 0 & 0 & 0 & 0 & 0 & 0 & 0 & 0 & F_1 & 0 \\ 0 & 0 & 0 & 0 & 0 & 0 & 0 & 0 & 0 & 0 & F_2 \\ 0 & 0 & 0 & 0 & 0 & 0 & 0 & 0 & 0 & 0 & 0 \\ 0 & 0 & 0 & 0 & 0 & 0 & 0 & 0 & 0 & 0 & 0 \\ 0 & 0 & 0 & 0 & 0 & 0 & 0 & 0 & 0 & F_3 & 0 \\ 0 & 0 & 0 & 0 & 0 & 0 & 0 & 0 & 0 & 0 & F_4 \\ 0 & 0 & 0 & 0 & 0 & 0 & 0 & 0 & 0 & 0 & 0 \\ 0 & 0 & 0 & 0 & 0 & 0 & 0 & 0 & 0 & 0 & 0 \\ 0 & 0 & F_5 & 0 & 0 & 0 & F_6 & 0 & 0 & 0 & 0 \\ 0 & 0 & 0 & 0 & F_7 & 0 & 0 & F_8 & 0 & 0 & 0 \end{pmatrix} \quad (2.4)$$

where:

$$\begin{aligned}
F_1 &= \frac{\beta_1 S}{V_0} & F_5 &= \frac{\alpha_1 V_0}{S + E_1 + E_2 + T_1 + T_2 + R} \\
F_2 &= \frac{\beta_2 S}{V_0} & F_6 &= \frac{\alpha_1 V_0}{S + E_1 + E_2 + T_1 + T_2 + R} \\
F_3 &= \frac{\sigma_1 \beta_1 T_2}{V_0} & F_7 &= \frac{\alpha_2 V_0}{S + E_1 + E_2 + T_1 + T_2 + R} \\
F_4 &= \frac{\sigma_2 \beta_2 T_1}{V_0} & F_8 &= \frac{\alpha_2 V_0}{S + E_1 + E_2 + T_1 + T_2 + R}
\end{aligned} \tag{2.5}$$

The ij th entry of F is the rate at which an individual in infected state j produces individuals with infected state i [13].

v is the vector formed by all the movements between the different classes in states $C_1, C_2, I_1, I_2, Z_1, Z_2, Y_1, Y_2, V_1, V_2$:

$$v = \begin{pmatrix} (\phi_1 + \mu) C_1 \\ (\phi_2 + \mu) C_2 \\ -\phi_1 C_1 + (\gamma_1 + \mu) I_1 \\ -\phi_2 C_2 + (\gamma_2 + \mu) I_2 \\ (\phi_1 + \mu) Z_1 \\ (\phi_2 + \mu) Z_2 \\ -\phi_1 Z_1 + (\gamma_1 + \mu + m_1) Y_1 \\ -\phi_2 Z_2 + (\gamma_2 + \mu + m_2) Y_2 \\ \delta V_1 \\ \delta V_2 \end{pmatrix} \tag{2.6}$$

Now V , given by the Jacobian of v , is:

$$V = \begin{pmatrix} u_1 & 0 & 0 & 0 & 0 & 0 & 0 & 0 & 0 & 0 \\ 0 & u_2 & 0 & 0 & 0 & 0 & 0 & 0 & 0 & 0 \\ u_3 & 0 & u_4 & 0 & 0 & 0 & 0 & 0 & 0 & 0 \\ 0 & u_5 & 0 & u_6 & 0 & 0 & 0 & 0 & 0 & 0 \\ 0 & 0 & 0 & 0 & u_7 & 0 & 0 & 0 & 0 & 0 \\ 0 & 0 & 0 & 0 & 0 & u_8 & 0 & 0 & 0 & 0 \\ 0 & 0 & 0 & 0 & u_9 & 0 & u_{10} & 0 & 0 & 0 \\ 0 & 0 & 0 & 0 & 0 & u_{11} & 0 & u_{12} & 0 & 0 \\ 0 & 0 & 0 & 0 & 0 & 0 & 0 & 0 & u_{13} & 0 \\ 0 & 0 & 0 & 0 & 0 & 0 & 0 & 0 & 0 & u_{14} \end{pmatrix} \tag{2.7}$$

where

$$\begin{aligned}
u_1 &= \phi_1 + \mu & u_2 &= \phi_2 + \mu \\
u_3 &= -\phi_1 & u_4 &= \mu + \gamma_1 \\
u_5 &= -\phi_2 & u_6 &= \mu + \gamma_2 \\
u_7 &= \phi_1 + \mu & u_8 &= \phi_2 + \mu \\
u_9 &= -\phi_1 & u_{10} &= \gamma_1 + \mu + m_1 \\
u_{11} &= -\phi_2 & u_{12} &= \gamma_2 + \mu + m_2 \\
u_{13} &= \delta & u_{14} &= \delta
\end{aligned} \tag{2.8}$$

The product $G = FV^{-1}$ evaluated in the disease-free equilibrium point give us the Next Generation Matrix G :

$$G = \begin{pmatrix} 0 & 0 & 0 & 0 & 0 & 0 & 0 & 0 & g_1 & 0 \\ 0 & 0 & 0 & 0 & 0 & 0 & 0 & 0 & 0 & g_2 \\ 0 & 0 & 0 & 0 & 0 & 0 & 0 & 0 & 0 & 0 \\ 0 & 0 & 0 & 0 & 0 & 0 & 0 & 0 & 0 & 0 \\ 0 & 0 & 0 & 0 & 0 & 0 & 0 & 0 & 0 & 0 \\ 0 & 0 & 0 & 0 & 0 & 0 & 0 & 0 & 0 & 0 \\ 0 & 0 & 0 & 0 & 0 & 0 & 0 & 0 & 0 & 0 \\ 0 & 0 & 0 & 0 & 0 & 0 & 0 & 0 & 0 & 0 \\ g_3 & 0 & g_4 & 0 & g_5 & 0 & g_6 & 0 & 0 & 0 \\ 0 & g_7 & 0 & g_8 & 0 & g_9 & 0 & g_{10} & 0 & 0 \end{pmatrix} \tag{2.9}$$

where:

$$\begin{aligned}
g_1 &= \frac{\beta_1 S}{V_0 \delta} & g_2 &= \frac{\beta_2 S}{V_0 \delta} \\
g_3 &= \frac{\alpha_1 V_0 \phi_1}{S(\phi_1 + \mu)(\mu + \gamma_1)} & g_4 &= \frac{\alpha_1 V_0}{S(\mu + \gamma_1)} \\
g_5 &= \frac{\alpha_1 V_0 \phi_1}{S(\phi_1 + \mu)(\mu + \gamma_1 + m_1)} & g_6 &= \frac{\alpha_1 V_0}{S(\mu + \gamma_1 + m_1)} \\
g_7 &= \frac{\alpha_2 V_0 \phi_2}{S(\phi_2 + \mu)(\mu + \gamma_2)} & g_8 &= \frac{\alpha_2 V_0}{S(\mu + \gamma_2)} \\
g_9 &= \frac{\alpha_2 V_0 \phi_2}{S(\phi_2 + \mu)(\mu + \gamma_2 + m_2)} & g_{10} &= \frac{\alpha_2 V_0}{S(\mu + \gamma_2 + m_2)}
\end{aligned} \tag{2.10}$$

The element G_{ij} is the expected number of new cases with state-at-infection i , generated by one individual who has just been born (epidemiologically speaking) in state-at-infection j [13].

The eigenvalues of the next generation operator are:

We equate the model (1.3) to zero and obtain

$$\begin{aligned}
\lambda - (B_1 + B_2)S - \mu S &= 0 \\
B_1S - (\phi_1 + \mu)C_1 &= 0 \\
B_2S - (\phi_2 + \mu)C_2 &= 0 \\
\phi_1C_1 - (\mu + \gamma_1)I_1 &= 0 \\
\phi_2C_2 - (\mu + \gamma_2)I_2 &= 0 \\
\gamma_1I_1 - (\mu + \eta_1)E_1 &= 0 \\
\gamma_2I_2 - (\mu + \eta_2)E_2 &= 0 \\
\eta_1E_1 - (\sigma_2B_2 + \mu)T_1 &= 0 \\
\eta_2E_2 - (\sigma_1B_1 + \mu)T_2 &= 0 \\
\sigma_1B_1T_2 - (\phi_1 + \mu)Z_1 &= 0 \\
\sigma_2B_2T_1 - (\phi_2 + \mu)Z_2 &= 0 \\
\phi_1Z_1 - (\gamma_1 + \mu + m_1)Y_1 &= 0 \\
\phi_2Z_2 - (\gamma_2 + \mu + m_2)Y_2 &= 0 \\
\gamma_1Y_1 + \gamma_2Y_2 - \mu R &= 0 \\
q(t) - (A_1 + A_2)V_0 - \delta V_0 &= 0 \\
A_1V_0 - \delta V_1 &= 0 \\
A_2V_0 - \delta V_2 &= 0
\end{aligned} \tag{2.13}$$

and, by taking only the two right parts of it, rewrite it as follows:

$$\begin{aligned}
S &= \frac{\lambda}{B_1 + B_2 + \mu} \\
C_1 &= \frac{B_1S}{\phi_1 + \mu} & C_2 &= \frac{B_2S}{\phi_2 + \mu} \\
I_1 &= \frac{\phi_1C_1}{\mu + \gamma_1} & I_2 &= \frac{\phi_2C_2}{\mu + \gamma_2} \\
E_1 &= \frac{\gamma_1I_1}{\mu + \eta_1} & E_2 &= \frac{\gamma_2I_2}{\mu + \eta_2} \\
T_1 &= \frac{\eta_1E_1}{\sigma_2B_2 + \mu} & T_2 &= \frac{\eta_2E_2}{\sigma_1B_1 + \mu} \\
Z_1 &= \frac{\sigma_1B_1T_1}{\phi_1 + \mu} & Z_2 &= \frac{\sigma_2B_2T_2}{\phi_2 + \mu} \\
Y_1 &= \frac{\phi_1Z_1}{\gamma_1 + m_1 + \mu} & Y_2 &= \frac{\phi_2Z_2}{\gamma_2 + m_2 + \mu} \\
R &= \frac{\gamma_1Y_1 + \gamma_2Y_2}{\mu} \\
V_0 &= \frac{q}{A_1 + A_2 + \delta} \\
V_1 &= \frac{A_1V_0}{\delta} & V_2 &= \frac{A_2V_0}{\delta}
\end{aligned} \tag{2.14}$$

We substitute the expressions in 2.14 and

$$N = S + C_1 + C_2 + I_1 + I_2 + E_1 + E_2 + T_1 + T_2 + Z_1 + Z_2 + Y_1 + Y_2 + R$$

$$M = V_0 + V_1 + V_2$$

in the forces of infection as they appear in chapter 1, equations 1.4 and 1.5.

Let $K = (A_1, A_2, B_1, B_2)'$ then we substitute the expressions given above (2.14) into the definitions of A_i and B_i to obtain a new system of four equations in terms of A_i and B_i .

From

$$A_1 = \frac{\alpha_1 (I_1 + Y_1)}{N}$$

$$A_i = \frac{\alpha_2 (I_2 + Y_2)}{N}$$

$$B_i = \frac{\beta_1 V_1}{M}$$

$$B_i = \frac{\beta_2 V_2}{M}$$

We obtain the system $K = \phi(K)$ (see appendix). The equation $K = \phi(K)$ allows the computation of the Next Generation Operator. We will obtain this operator by calculating the Jacobian of ϕ at the disease-free equilibrium point. The operator will look as follows:

$$\begin{pmatrix} 0 & 0 & \frac{\alpha_1 \phi_1}{(\phi_1 + \mu)(\gamma_1 + \mu)} & 0 \\ 0 & 0 & 0 & \frac{\alpha_2 \phi_2}{(\phi_2 + \mu)(\gamma_2 + \mu)} \\ \frac{\beta_1}{\delta} & 0 & 0 & 0 \\ 0 & \frac{\beta_2}{\delta} & 0 & 0 \end{pmatrix} \quad (2.15)$$

The eigenvalues of next generation operator are:

$$\begin{pmatrix} \sqrt{\frac{\phi_2 \beta_2 \alpha_2}{\delta (\gamma_2 + \mu) (\phi_2 + \mu)}} \\ -\sqrt{\frac{\phi_2 \beta_2 \alpha_2}{\delta (\gamma_2 + \mu) (\phi_2 + \mu)}} \\ \sqrt{\frac{\phi_1 \beta_1 \alpha_1}{\delta (\gamma_1 + \mu) (\phi_1 + \mu)}} \\ -\sqrt{\frac{\phi_1 \beta_1 \alpha_1}{\delta (\gamma_1 + \mu) (\phi_1 + \mu)}} \end{pmatrix} \quad (2.16)$$

We will name

$$\begin{aligned}
R_0^1 &= \left| \sqrt{\frac{\phi_1 \beta_1 \alpha_1}{\delta (\gamma_1 + \mu) (\phi_1 + \mu)}} \right| \\
R_0^2 &= \left| \sqrt{\frac{\phi_2 \beta_2 \alpha_2}{\delta (\gamma_2 + \mu) (\phi_2 + \mu)}} \right|
\end{aligned} \tag{2.17}$$

R_0^1 is the basic reproductive number where only strain 1 is involved and strain 2 has no influence in it while R_0^2 is the opposite with no influence of strain 1 in it.

The Basic Reproductive Number is the spectral radius of the Next Generation Operator (2.3.2).

$$R_0 = \max \left\{ \left| \sqrt{\frac{\phi_1 \beta_1 \alpha_1}{\delta (\gamma_1 + \mu) (\phi_1 + \mu)}} \right|, \left| \sqrt{\frac{\phi_2 \beta_2 \alpha_2}{\delta (\gamma_2 + \mu) (\phi_2 + \mu)}} \right| \right\}$$

2.4 Some Conclusions on the Basic Reproductive Number

Now we have the estimation for the basic reproductive number R_0 . R_0 is given by an expression of the form:

$$\sqrt{\frac{\phi_i \beta_i \alpha_i}{\delta (\gamma_i + \mu) (\phi_i + \mu)}} \tag{2.18}$$

for $i = 1, 2$.

We observe in the expression the product of three quantities inside the square root.

Commonly in the basic reproductive number we have involved the infection rate in the numerator while the denominator contains the healing rate and for this case it is no exception to that, R_0 involves the product of three parameters in the numerator: one is the rate of effective contact mosquito to human (β), the second is the other rate of effective contact, this time human to mosquito (α), and the third involved in the numerator is the inverse of the duration of the incubation period (ϕ). The three parameters are strongly related to the infection rate. β and α will determine the speed of the contagium in the model.

In the denominator we have the product of also three quantities: one is the inverse of life expectance for mosquitoes (δ); other factor is the sum of the inverse of the duration of the incubation period (ϕ) and the inverse of life expectance for humans (μ); and the last factor is the sum of the inverses of the duration of the disease (γ) and life expectance for humans (μ).

Thus the expression we obtained for R_0 give us a value which will allow us to categorize the impact of the disease in the population. It is the square root of the product of the following three main quantities:

$$\left(\frac{\beta_i}{\delta}\right) \left(\frac{\alpha_i}{\gamma_i + \mu}\right) \left(\frac{\phi_i}{\phi_i + \mu}\right)$$

They can be interpreted as follows. $\frac{\beta_i}{\delta}$, represents the number of effective contacts mosquito-to-human during the life time of mosquito. $\frac{\alpha_i}{\gamma_i + \mu}$, represents the number of effective contact human-to-mosquito during the infectious period of human. And, $\frac{\phi_i}{\phi_i + \mu}$ represents the fraction of time a human remains in the incubation period of the disease.

Finally, we have an expression for R_0 , the threshold parameter for the model, such that if $R_0 < 1$ the disease cannot invade the population (eventually the infection dies out), but if $R_0 > 1$, then the Disease will invade the population. In the next chapter, we will explore the space of parameters.

Chapter 3

Numerical Studies

In the previous chapter we have calculated the expression for R_0 . This important number helps us to identify in what cases there will be an epidemic outbreak in the population we are studying. The value R_0 takes depends on other parameters so now we want to study those parameters.

We have to deal with 17 parameters in the system we are studying (1.3), this makes the study very complex to do it fully. For simplicity, we will take into consideration that these parameters are known to be in a range of determined values. Also, in this chapter we will study β_i through a bifurcation analysis by setting the rest of parameters to acceptable numeric values in their range of definition. β_i ($i=1,2$) is the effective contact rate mosquito-to-human. From the human point of view β_i is the most important parameter involved in the model because it is the one that measures the appearance of new infections among humans. With the results of the graphical bifurcation analysis of β_i we will define four regions of interest to study the model (1.3).

Based in the results of these analysis (of R_0 and the bifurcation of β_i) we will proceed to present, in this chapter, some simulations of the model (1.3) by solving it and presenting the time series obtained at each region of interest. These simulations will be used in the analysis of data with the use of wavelets in chapter 4.

3.1 Bifurcation Analysis for β_i

This type of analysis will provide information on the dependence of the parameters.

Figure 3.1A shows a transcritical bifurcation for parameters β_1 and β_2 using the case I of the model (1.3). They were obtained with the use of tool Auto of software XPPAUT [54].

The transcritical bifurcation only happens when the system has an equilibrium that exists regardless of the values of the parameters and cannot be destroyed in a neighborhood. When this equilibrium collides with another equilibrium, the two equilibria exchange their stability properties, but continue to exist both before and

after the collision. Hence, the two equilibria pass through each other. [41].

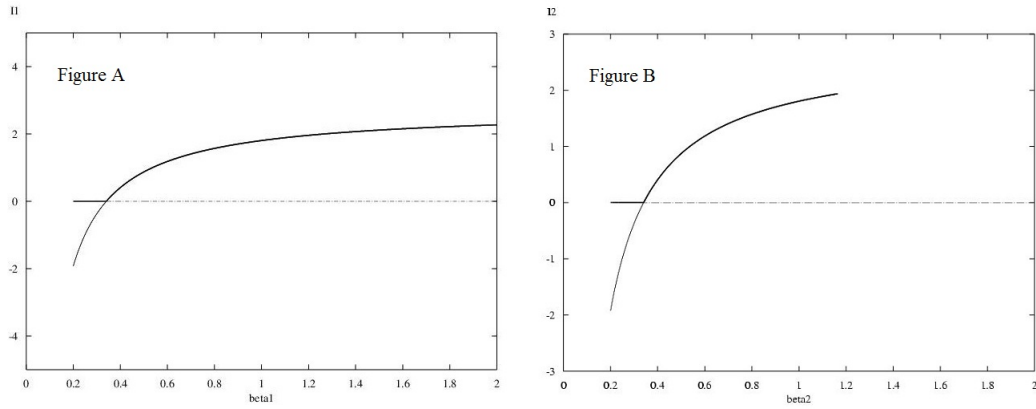


Figure 3.1: Figure A: Transcritical Bifurcation β_1 . Figure B: Transcritical Bifurcation for β_2 .

Notice that the parameters of strain 1 does not influence in any way to strain 2 and viceversa. This can easily be seen in the expression we have obtained for R_0 in Chapter 2.

The bifurcation point can be found by equating the model 1.3 to zero, and solving for all the variables of interest. With the help of software we found three different solutions. As we are interested in those having biological sense, we will take into considerations only two:

$$(S^{*1}, C_1^{*1}, C_2^{*1}, I_1^{*1}, I_2^{*1}, E_1^{*1}, E_2^{*1}, T_1^{*1}, T_2^{*1}, Z_1^{*1}, Z_2^{*1}, Y_1^{*1}, Y_2^{*1}, R^{*1}, V_0^{*1}, V_1^{*1}, V_2^{*1})$$

$$= \left(\frac{\lambda}{\mu}, 0, \dots, 0, \frac{q}{\delta}, 0, 0 \right)$$

and

$$(S^{*2}, C_1^{*2}, C_2^{*2}, I_1^{*2}, I_2^{*2}, E_1^{*2}, E_2^{*2}, T_1^{*2}, T_2^{*2}, Z_1^{*2}, Z_2^{*2}, Y_1^{*2}, Y_2^{*2}, R^{*2}, V_0^{*2}, V_1^{*2}, V_2^{*2})$$

where

$$\begin{aligned}
S^{*2} &= \frac{\lambda (\delta \gamma_1 \phi_1 + \alpha_1 \mu \phi_1 + \delta \mu^2 + \delta \mu \phi_1)}{\mu \phi_1 \alpha_1 (\mu + \beta_1)} \\
C_1^{*2} &= \frac{-\lambda (\delta (\gamma_1 + \mu) (\phi_1 + \mu) - \beta_1 \phi_1 \alpha_1)}{\phi_1 \alpha_1 (\beta_1 \phi_1 + \beta_1 \mu + \mu^2 + \mu \phi_1)} \\
I_1^{*2} &= \frac{-\lambda (\delta (\gamma_1 + \mu) (\phi_1 + \mu) - \beta_1 \phi_1 \alpha_1)}{\alpha_1 (\beta_1 \gamma_1 \phi_1 + \beta_1 \mu^2 + \beta_1 \gamma_1 \mu + \phi_1 \mu \beta_1 + \mu^2 \gamma_1 + \mu^2 \phi_1 + \mu \mu \phi_1 \gamma_1 + \mu^3)} \\
E_1^{*2} &= -\gamma_1 \lambda (\delta (\gamma_1 + \mu) (\phi_1 + \mu) - \beta_1 \phi_1 \alpha_1) \alpha_1^{-1} \dots \\
&\quad (\phi_1 \gamma_1 \eta_1 \mu + \mu \gamma_1 \eta_1 \beta_1 + \gamma_1 \mu \phi_1 \beta_1 + \mu^3 \beta_1 + \mu^2 \eta_1 \phi_1 + \gamma_1 \eta_1 \mu^2 + \mu^3 \phi_1 + \mu^3 \eta_1 + \dots \\
&\quad \mu^3 \gamma_1 + \mu^2 \gamma_1 \phi_1 + \mu^2 \phi_1 \beta_1 + \mu^2 \eta_1 \beta_1 + \mu^2 \gamma_1 \beta_1 + \mu \eta_1 \phi_1 \beta_1 + \gamma_1 \phi_1 \eta_1 \beta_1 + \mu^4)^{-1} \\
T_1^{*2} &= -\eta_1 \gamma_1 \lambda (\delta (\gamma_1 + \mu) (\phi_1 + \mu) - \beta_1 \phi_1 \alpha_1) \alpha_1^{-1} \dots \\
&\quad (\phi_1 \gamma_1 \eta_1 \mu + \mu \gamma_1 \eta_1 \beta_1 + \gamma_1 \mu \phi_1 \beta_1 + \mu^3 \beta_1 + \mu^2 \eta_1 \phi_1 + \gamma_1 \eta_1 \mu^2 + \mu^3 \phi_1 + \mu^3 \eta_1 + \dots \\
&\quad \mu^3 \gamma_1 + \mu^2 \gamma_1 \phi_1 + \mu^2 \phi_1 \beta_1 + \mu^2 \eta_1 \beta_1 + \mu^2 \gamma_1 \beta_1 + \mu \eta_1 \phi_1 \beta_1 + \gamma_1 \phi_1 \eta_1 \beta_1 + \mu^4)^{-1}
\end{aligned}$$

and the rest are zero.

Table 3.1: Parameters used to calculate the value of bifurcation in β_1 .

Parameter	Description	Values
δ^{-1}	life expectance of mosquitoes	21 days
γ_1^{-1}	Duration of disease strain 1	7 days
ϕ_1^{-1}	Incubation period strain 1	7 days
α_1	Rate of effective contact host to vector	0.02
μ^{-1}	Human life expectance	0.0000391389
λ	Incoming population	0.391389432

To find an expression of the bifurcation point for β_1 in terms of the rest of parameters, we equate $S^{*1} = S^{*2}$ and we solve for β_1 . We obtain:

$$\beta_i = \frac{\delta (\gamma_1 + \mu) (\phi_1 + \mu)}{\phi_1 \alpha_1} \quad (3.1)$$

Note that any other entry of the solutions can be used as they all would lead to the same expression for β_1 . For example, we can use $C_1^{*1} = C_1^{*2}$, $I_1^{*1} = I_1^{*2}$, $E_1^{*1} = E_1^{*2}$, or $T_1^{*1} = T_1^{*2}$.

3.1.1 Analysis of the bifurcation value for β_i in terms of R_0

Using the expression obtained in previous for β_1 (3.1) and with the values of the parameters in table (3.1) we obtain $\beta_1 = 0.3402$ as the bifurcation point. This means

that the value $\beta_1 = 0.3402$ is a threshold and we want to see what happens with R_0 when β_1 is below its threshold or up it.

The expression for R_0 is given by

$$R_0 = \max \{ |R_0^1|, |R_0^2| \}$$

(refer to calculations on chapter 2, results in 2.3.2).

Changing the parameters for the known values shown in table (3.1), we obtain the following expression for R_0^1 :

$$R_0^1 = 1.432356037\beta_1^{\frac{1}{2}}$$

From this last expression we can easily observe the effects that the variation of the value of β_1 has in the value of R_0 , as we show in the table (3.2).

Table 3.2: Effect of variations in β_1 using parameters given in table (3.1).

Value of β_1	Description	Value of R_0^1
0.1	below the threshold	0.6648407789 (less than 1)
0.3	below the threshold	0.9588663277 (less than 1)
0.3402887023	threshold	1.000000368
0.35	up the threshold	1.009424089 (greater than 1)
0.6	up the threshold	1.208095870 (greater than 1)

As we can see the value of β_1 will directly influence on R_0 and this is the value that will determine if the system will reach an equilibrium state or not. This shows that there is a change of stability when passing through the bifurcation point $\beta_1 = 0.3402$.

Since the same analysis can be made around β_2 to find another transcritical bifurcation and from that getting the conclusion that β_2 will influence on R_0^2 , then we can conclude that both values, β_1 and β_2 , are determinant for R_0 , as it will depend on them.

3.2 Regions

3.2.1 Parameters

The parameters used in the simulations were set with the values shown in table (3.3). The values were chosen from Velasco-Feng studies [17] and [51].

Table 3.3: Chosen values of parameters.

Parameter	Description	Values
$\frac{1}{\mu}$	Life expectance for humans	25500 days
λ	Incoming population	0.391389432
$\frac{1}{\phi_1}$	Incubation period	7 days
$\frac{1}{\phi_2}$	Incubation period	4 days
$\frac{1}{\gamma_1}$	Duration of disease	7 days
$\frac{1}{\gamma_2}$	Duration of disease	15 days
$\frac{1}{\delta}$	Life expectance of mosquitoes	21 days
$\frac{1}{\eta_1}$	Duration of Crossed immunity	20 days
$\frac{1}{\eta_2}$	Duration of Crossed immunity	20 days
σ_i	Reinfection rate	1
α_1	Rate of effective contact human to mosquito	0.02
α_2	Rate of effective contact human to mosquito	0.03

3.2.2 Regions

Four regions are of interest since they refer to cases where $R_0 > 1$ and there could be an epidemic.

Since R_0^1 represents the value of the basic reproductive number where only strain 1 is involved as calculated in the previous chapter, and R_0^2 is the value where only strain 2 is involved as we calculated before (see 2.3.2); we can separate the four regions as shown in table (3.4):

Table 3.4: Regions of study for the model (1.3) to be analyzed in the following section.

Regions	Case of study	Values of β_i	R_0 obtained
Region I:	$R_0^2 < 1 < R_0^1 = R_0$	$\beta_1 = 3, \beta_2 = 0.05$	$R_0 = 2.969183$
Region II:	$R_0^1 < 1 < R_0^2 = R_0$	$\beta_1 = 0.06, \beta_2 = 1.5$	$R_0 = 3.76434$
Region III:	$1 < R_0^2 < R_0^1 = R_0$	$\beta_1 = 3, \beta_2 = 0.7$	$R_0 = 2.96918$
Region IV:	$1 < R_0^1 < R_0^2 = R_0$	$\beta_1 = 2.5, \beta_2 = 1.3$	$R_0 = 3.504412$

These regions represent the four cases of interest in which we want to simulate the model (1.3). We have used the values of parameters as given in table (3.3). In all of them we have $1 \leq R_0$ which implies the appearance of an epidemic.

Region I represents the case where only strain 1 exists in the population while Region II represents the case where only strain 2 exists in the population. These regions place one of the reproductive numbers below one and the other above. Both cases represent an endemic equilibrium for the system (1.3). In the first region we have R_0 determined by R_0^1 , which gives a significant advantage to strain 1 over strain

2 (whose $R_0^2 < 1$). The second region is the opposite to the first, here $R_0 = R_0^2$ and it is greater than one, while R_0^1 is below one.

Region III represents the case where both strains coexist in the endemic equilibrium being strain 1 stronger than strain 2 as pointed by the given values of R_0 in table (3.4). The region III shows the case where R_0^1, R_0^2 are both greater than 1; also in this case we gave preference to strain 1 over strain, this time R_0 coincides with R_0^2 .

Region IV represents another case where both strains coexist but strain 2 is stronger than strain 1 (see table (3.4)). Region IV shows a case which differs from region III in that it gives preference to strain 2 over strain 1 that we can notice when we see that R_0 coincides this time with R_0^2 .

We have selected this four regions based in the biological interest they offer. From a mathematical point of view some cases may look repetitive but they are not the same from a biological point of view since we are dealing with two different strains of a disease. In the following sections we will analyze what happens in each region based on the simulations done.

3.2.3 Initial Conditions

The initial conditions we choose for populations are shown in the table (3.5) and they will provide the scenario for the simulations.

Table 3.5: Initial Values that took to run the Simulations.

Human Host	Values
S	10 000
$C_1, C_2, I_1, I_2, E_1, E_2, T_1, T_2, Z_1, Z_2, Y_1, Y_2, R$	0
Mosquitoes	Values
V_0	300
V_1	55
V_2	15

3.3 Simulations

We present the simulations we have done in the four regions we have defined. Each region is separated in two cases depending on the value of $q(t)$, the incoming mosquitoes into the susceptible population of mosquitoes: one for the autonomous model (making $q(t) = 1$), where we assume that the dynamics of the disease is independent of the environment; and the other for the seasonality case (making $q(t) = 1 + \cos(2\pi t/365)$), where we consider the effects of a one year longed cycle in the dynamics of dengue. We present first the autonomous cases and after each of

them its seasonality case for the region.

3.3.1 Region I - Autonomous Case

Region I represents the case where only strain 1 exists in the population. It is the case where $R_0 = R_0^1 > 1 > R_0^2$, $\beta_1 = 3, \beta_2 = 0.05$, $R_0 = 2.969183$.

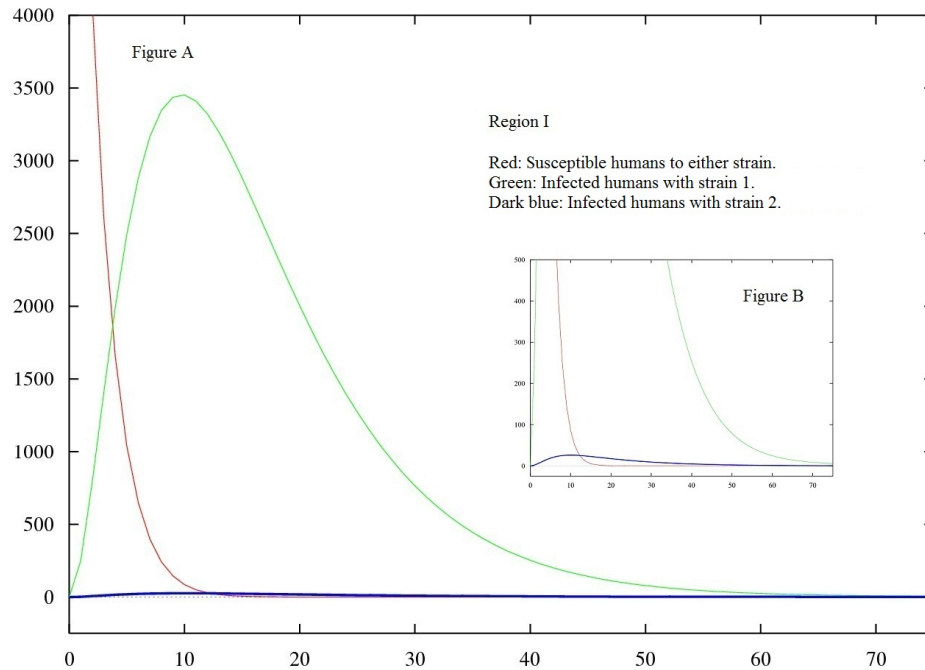


Figure 3.2: Y-axis: the number of humans. X-axis: time from 0 to 70 days. Red: Human Susceptible to either strain. Green: First time infected humans with strain 1 (stage I_1). Dark blue: First time infected humans with strain 2 (stage I_2). Figure A: Shows how the number of susceptibles decreases while the number of first time infected is increasing. Infected with strain 1 gains in number while those infected with strain 2 grow a bit to later disappear. Figure B: A more detailed view to the behavior of strain 2.

In the first 70 days, the simulations show that both strains are present but only a very short time. Then, strain 2 disappears totally under the effect caused by strain 1 (see figures (3.2) and (3.3)). Notice that since we have $R_0^2 < 1$ it implies that there is a bigger number of infected humans with strain 1 than with strain 2. Also, we observe that both strains coexist in the lapse of time.

We are interested in seeing what happens in bigger lapses of time so, we continued the simulation for 68 years (25000 days), and we obtained figure 3.3. In this figure we can see that the number of humans infected with strain 1 (stage I_1) oscillates between 0 and 92 for the time observed among 15000 to 25000 days. Figures

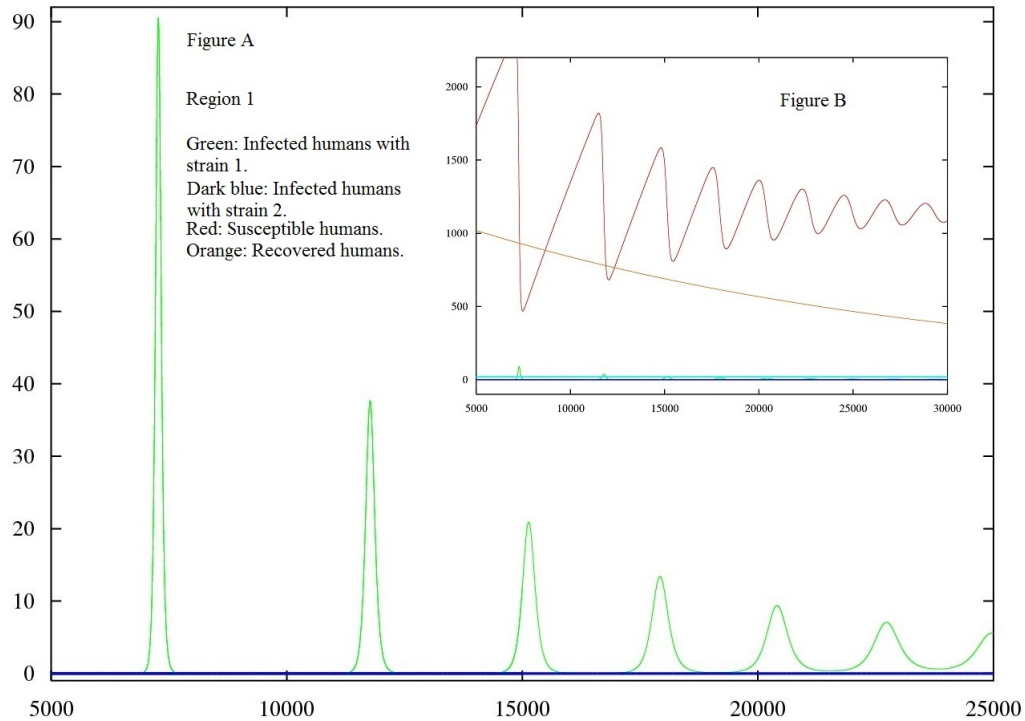


Figure 3.3: Y-axis: the total amount of humans. X-axis: time from 5000 (13 years) to 25000 (68 years). Figure A: The green curve represents the number of infected humans with strain 1 and the dark blue curve the number of humans infected with strain 2. Figure B: The red curve of susceptible humans oscillates. The orange curve represents the number of humans in the recovered stage

3.3A and 3.3B show stages S , I_1 , I_2 and R , in red, green, dark blue and orange color respectively. Notice that susceptibles are also oscillating which was not evident in figure 3.2. From figure 3.3B we can see that oscillations of stage S of susceptibles are damped and the number of individuals in the R stage of recovered humans is decreasing. When we continue the simulation for a larger lapse of time we observe that the curve for the number of recovered humans, R , converges asymptotically to a positive value different from zero.

The curve representing humans that are first time infected and get strain 1 (stage I_1) oscillates (see green curve in figure 3.3A). The amplitude of the oscillations for I_1 is very small in comparison with the red curve of susceptibles (see figure 3.3B) which has a wider oscillation. The humans that get the disease for the first time and are infected with strain 2 (stage I_2) get reduced to zero very quickly and remains there for all future time (see the dark blue curve in figure 3.3B).

To get a better understanding of what causes the oscillations, we present the dynamics of mosquitoes for the same time intervals in figures 3.4 and 3.5.

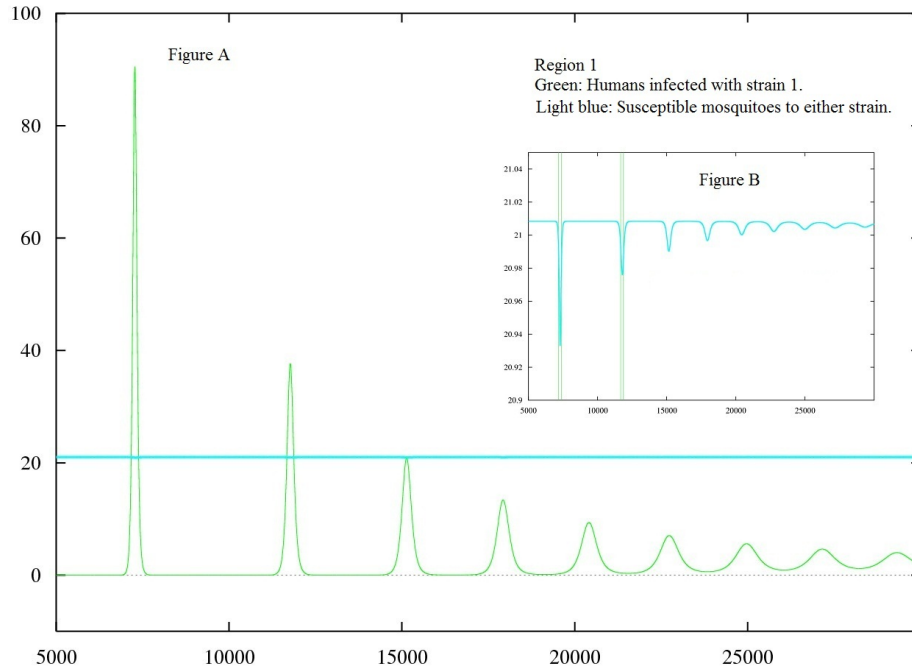


Figure 3.4: Y-axis: number of individuals. X-axis: Time in days from 5000 (13 years) to 25000 (68 years). Figure A: The green curve represents the number of humans infected with strain 1 at a time t . The light blue curve of susceptible mosquitoes seems to be at equilibrium with 21.0084 mosquitoes. Figure B: The light blue curve of susceptible mosquitoes also oscillates at the same time as the curve for infected humans that is shown in green.

When we observe the stage for susceptible mosquitoes, with V_0 as the light blue curve it looks like a straight line due to the scale 3.4A). But when we make zoom around $y = 21$ (see figure 3.4B), we have oscillations for stage V_0 . In figure 3.5B, we also observe oscillations for stage V_1 (red curve). For V_2 nothing interesting happens since it dies almost from the beginning, as strain 1 is the only that survives.

The light blue curve for V_0 (see figure 3.4) represents the number of susceptible mosquitoes present in the population at a given time. We can see that the number of susceptible mosquitoes remain mostly stable at $y = 21.0084$ except for the moments when the curve goes down, each time mosquitoes get infected by strain 1. After the number of susceptible mosquitoes increases, the curve reaches back the value $y = 21.0084$.

In figure 3.5B, the red curve for V_1 is very similar to the green curve for I_1 but in a smaller scale. We can see in figure 3.5B that each time the number of infected humans increases it is followed by an increment of the number of infected mosquitoes. Mosquitoes grow in number in a lower scale than humans but seems that both reach their highest point at the same time. Then both, mosquitoes and humans, begin to

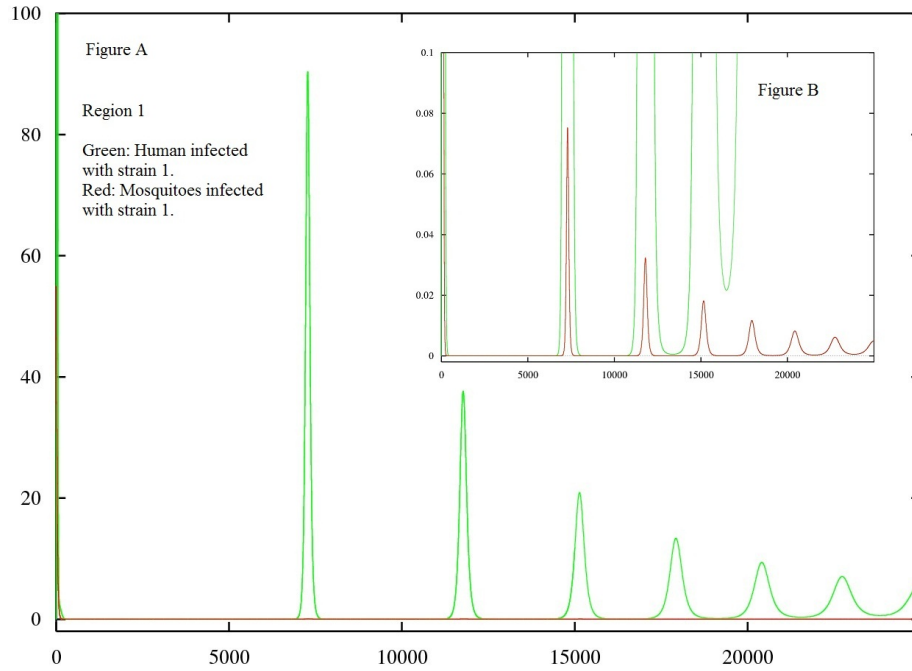


Figure 3.5: Y-axis: number of individuals. X-axis: Time in days from 0 to 25000 (68 years). Figure A: Stages I_1 for infected humans (green) and V_1 for infected mosquitoes (red). Figure B: Close up view from figure A.

decrease their number of infected. Mosquitoes start to decrease and are followed by humans.

Resuming, initially, there are 55 mosquitoes infected with strain 1, and 35 mosquitoes infected with strain 2. As they get in contact with the population, the number of susceptible humans decreases and the number of first time infected increases. $R_0^1 = 2.9$ which indicates that in average each individual infected will pass the disease strain 1 to about 3 other individuals in the course of one generation. Meanwhile, $R_0^2 = 0.6 < 1$ tells us that the strain 2 of the disease will eventually disappear from the population.

In the first 10 days (figure 3.2), humans are getting infected with strain 1 very fast. After the 10th day, many in the population will be already infected with strain 1 and this will make it hard for mosquitoes to find "clean individuals" to infect. Then, the number of new infections reduces. Several humans in the population will soon be immune to strain 1 and there will be an interval of time where strain 1 remains very "quiet". Later, susceptibles increase due to new incoming individuals, and there will be enough susceptible humans again for the disease to spread among the population. The number of infected individuals will increase once more until the population is saturated with infected humans of strain 1. This behavior causes

the oscillations we observed in the figures 3.2 - 3.5. Because the population still alive is gaining immunity and the number of humans in the population must remain constant at all times, the oscillations are damped.

3.3.2 Region I - Seasonality Case

Region I represents the case where only strain 1 exists in the population. It is the case where $R_0 = R_0^1 > 1 > R_0^2$, $\beta_1 = 3, \beta_2 = 0.05$, $R_0 = 2.969183$. This is the simulation for the seasonality case.

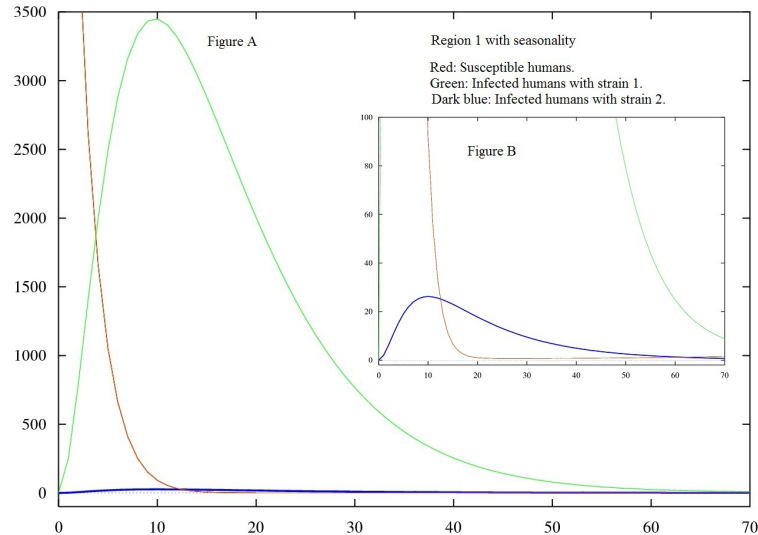


Figure 3.6: Y-axis: the number of humans. X-axis: time from 0 to 70 days. Red: Human Susceptible to either strain. Green: First time infected humans with strain 1 (stage I_1). Dark blue: First time infected humans with strain 2 (stage I_2). Figure A: Shows how the number of susceptibles decreases while the number of first time infected is increasing. Infected with strain 1 gains in number while those infected with strain 2 grow a bit to later disappear. Figure B: A more detailed view to the behavior of strain 2.

Figure 3.6 shows that in the beginning the behavior of the seasonality case does not differ very much from the autonomous case. We can see in it that in the first 70 days susceptible humans are decreasing as the number of infected increases. Also, we note that both strains coexist in this period of 70, but strain 2 infects less humans and it disappears soon after this period of 70 days.

Even oscillations for I_1 and V_1 are present in this seasonal case as in the autonomous case, we observe differences in the oscillations of the curves as many peaks appear now in between the high outbreaks (figure 3.7). To explain this we must first see the curve for the stage of susceptible mosquitoes (V_0) in figure 3.8.

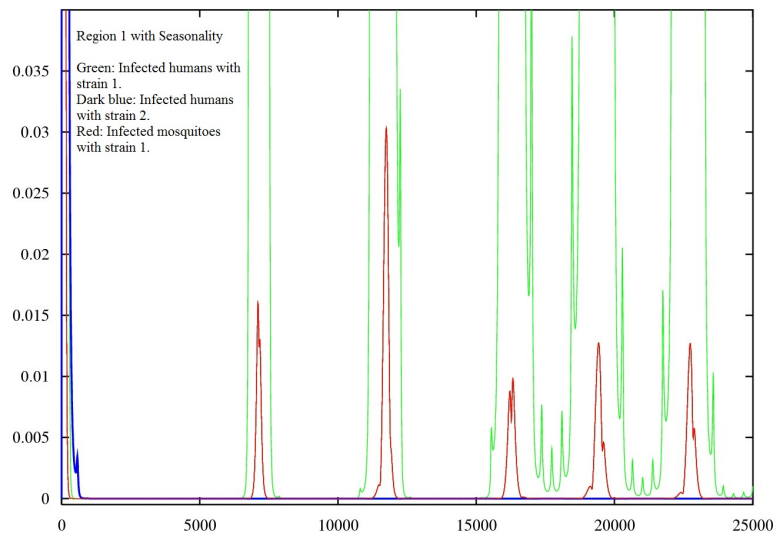


Figure 3.7: Y-axis: the number of humans. X-axis: time from 0 to 25000 days (68 years). Green: First time infected humans with strain 1 (stage I_1). Red: Mosquitoes infected with strain 1 (stage V_1). The figure shows the oscillations of stages I_1 and V_1 , both occurring at same instants of time but at different magnitudes.

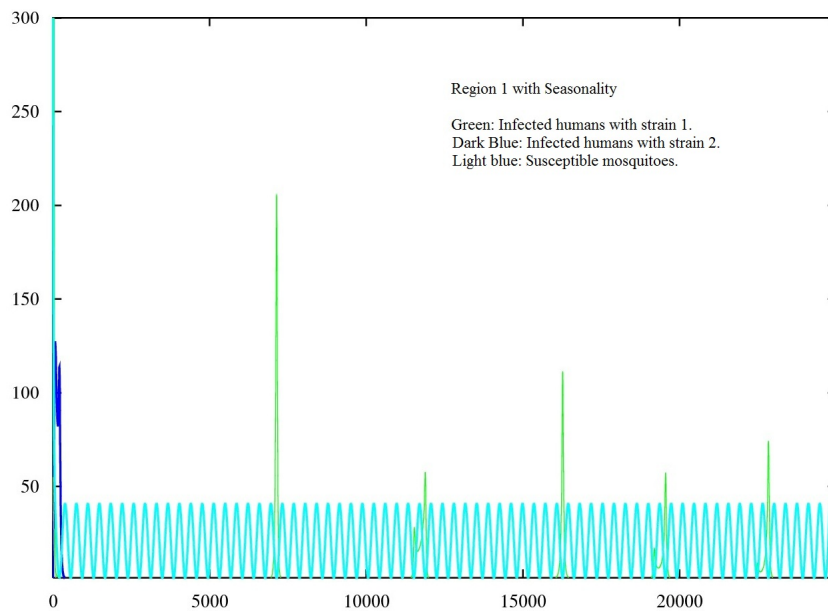


Figure 3.8: Y-axis: the number of humans. X-axis: time from 0 to 25000 days (68 years). Green: First time infected humans with strain 1 (stage I_1). Dark blue: First time infected humans with strain 2 (stage I_2). Light blue: Susceptible mosquitoes (stage V_0). Figure shows the behavior of susceptible stage of mosquitoes when new mosquitoes arrive not in constantly but in a quantity given by $q(t) = 1 + \cos(2\pi t/365)$.

This time the curve for stage V_0 decreases in the beginning until it establishes in a perpetual oscillation in a band among the values of $y = 0$ and $y = 50$ (see light dark blue curve in figure 3.8). As we said before, the difference between the seasonality and the autonomous case is the value for the incoming individuals into the mosquito population. For the seasonality case, we have set the entrance of mosquitoes as $q(t) = 1 + \cos(2\pi t/365)$. This produces the oscillation in the number of susceptible mosquitoes that we see in figure 3.8.

We show a closer graph of one of the outbreaks in figure 3.9A where we observe better the many peaks in one outbreak of figure 3.3. At $t = 11400$, mosquitoes are decreasing each time slower, while infected humans (in stage I_1) are increasing each time faster. By the time mosquitoes reach their lowest, infected humans reach a maximum and start to decrease (because although conditions are good, there are not enough mosquitoes to get the disease and spread it). Then, the season of growing arrives for mosquitoes and there are each time more mosquitoes in the population. Then the infected human begin to increase again. As this happens, we observe the stage of susceptible humans (S), shown in figure 3.9B, that is decreasing as humans get infected.

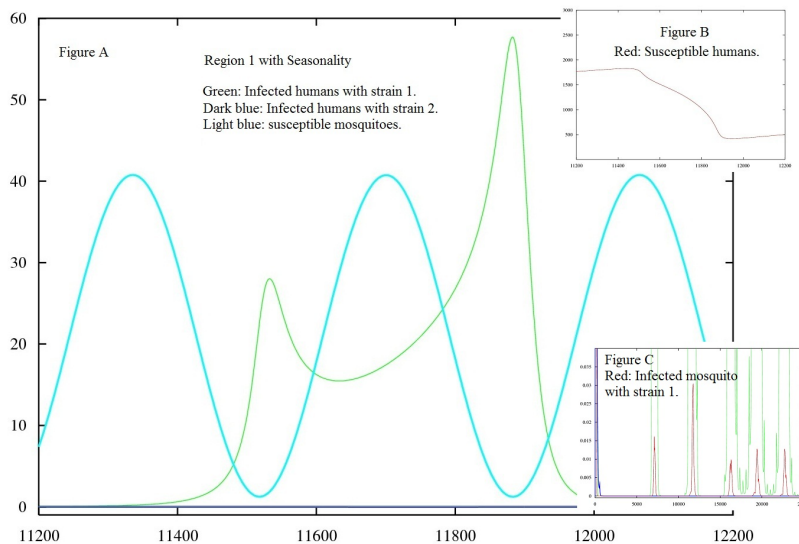


Figure 3.9: Y-axis: the number of humans. X-axis: time from 11200 (30 years) to 12200 days (33 years). Red: Human Susceptible to either strain (stage S). Green: First time infected humans with strain 1 (stage I_1). Light blue: Susceptible mosquitoes to either strain (stage V_0). Figure A: Detailed view from figure 3.8. Susceptible mosquitoes oscillate while the number of human infected shows a two-peaked outbreak. Figure B: Shows how the number of susceptibles decreases while the number of first time infected is increasing.

3.3.3 Region II - Autonomous Case

Region II represents the case where only strain 2 exist in the population. In this case we have $R_0^1 < 1 < R_0^2 = R_0$, $\beta_1 = 0.06$, $\beta_2 = 1.5$ and $R_0 = 3.76434$. This case

is the analogous for region I, but here strain 2 is stronger and it is the one that oscillates, while strain 1 disappears.

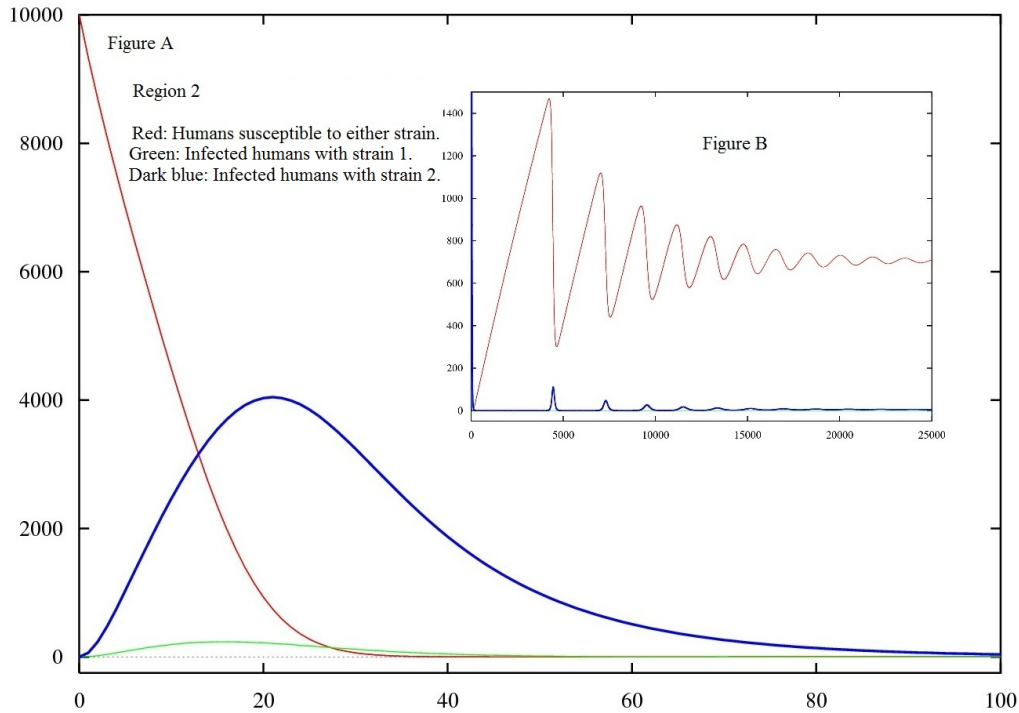


Figure 3.10: Y-axis: number of humans. Figure A: behavior of stages S , I_1 , and I_2 in the first 100 days. Figure B: Zoom out view of Figure A from day 0 to 25000 (68 years).

Initially, we can observe in figure 3.10 that the number of susceptibles is decreasing while the number of infected grows. We see that, with $R_0^2 = 3.76$, strain 2 can infect more than 3 humans in one generation, while strain 1, with $R_0^1 = 0.41 < 1$ soon disappears from population as it was expected.

In the beginning, humans get infected with either strain causing the number of humans at stage S of susceptibles to decrease. Since $R_0^2 = 3.76$, stage I_2 grows very fast infecting humans, while stage I_1 for strain 1 also increases but it causes fewer infections. In figure 3.11, we can notice that as the number of humans infected with strain 2 grows there are less susceptible to infect and, although it is easier for mosquitoes to get infected with strain 2 ($R_0^2 > 1$), it becomes more difficult for mosquitoes to pass it to a human, as most humans are already infected!

This situation force to a reduction in the number of humans infected with strain 2 and causes a "pause" where the disease seems to have almost disappear. But this pause will only last till the incubation time and the duration of the disease for strain 1 in humans have passed, and new susceptibles had arrive into the population. This will create one more time the scenario for another increment in the number of in-

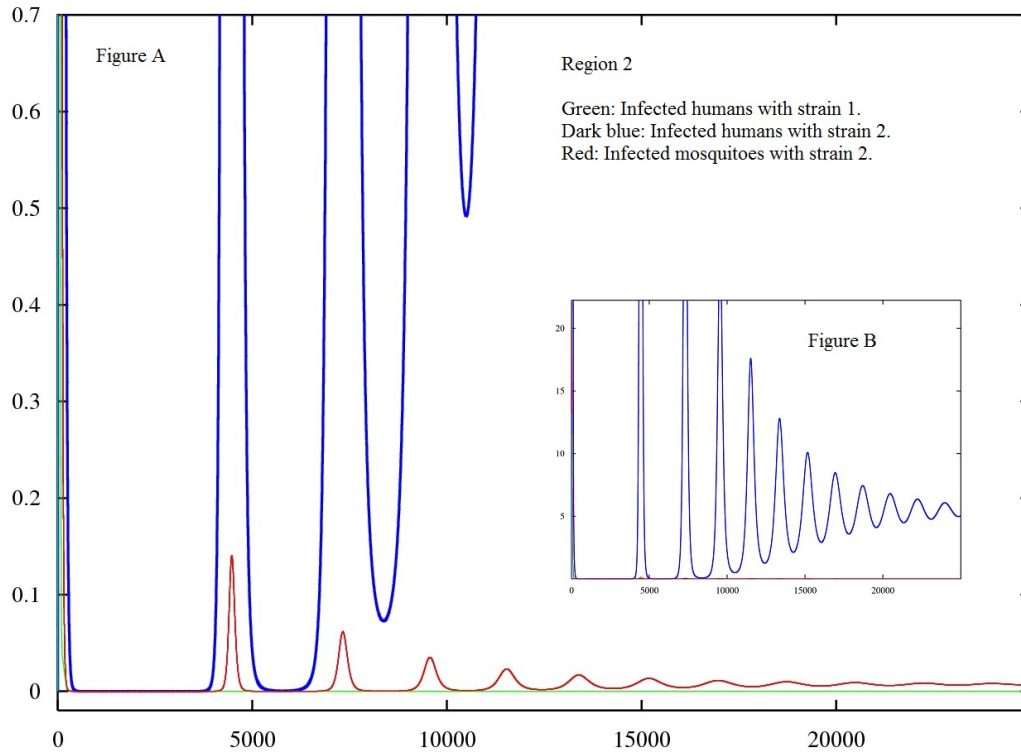


Figure 3.11: Y-axis: number of humans. X-axis: time for day 0 to 25000 (68 years). Figure A: behavior of stages I_2 , and V_2 . Figure B: Zoom out view of Figure A showing the oscillations of I_2 .

ected of strain 2 in the population. And the events repeat themselves again causing the oscillations we see in the figures. Note that oscillations are decreasing each time.

3.3.4 Region II - Seasonality Case

Region II represents the case where only strain 2 exist in the population. In this case we have $R_0^1 < 1 < R_0^2 = R_0$, $\beta_1 = 0.06, \beta_2 = 1.5$ and $R_0 = 3.76434$. This case is the analogous for region I, only here strain 2 is stronger than strain 1 and it is the one that oscillates, while strain 1 disappears. This is the seasonality case were we assumed that new mosquitoes arrive to the susceptible population at a rate $q(t) = 1 + \cos(2\pi t/365)$ which depends on time.

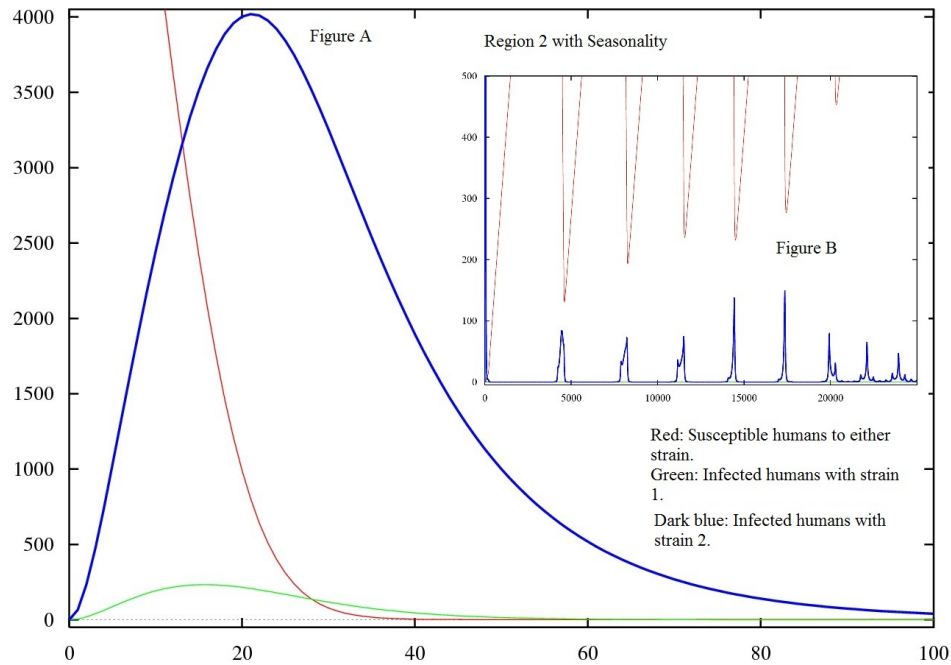


Figure 3.12: Y-axis: the number of humans. X-axis: time of the first 100 days of the disease. Red: Human Susceptible to either strain (stage S). Green: First time infected humans with strain 1 (stage I_1). Dark blue: First time infected humans with strain 2 (stage I_2). Figure A: The number of susceptible humans, S , decreases as the number of infected, I_1 and I_2 , increases. Figure B: Shows how the number of susceptibles oscillates while the number of first time infected with strain 2 oscillates. Strain 1 has disappeared from the population.

Figure 3.12A shows the first 100 days of the simulation. We have that both strains coexist, stages I_1 and I_2 , show both an outbreak that causes the number of susceptible to decrease, stage S . While in figure 3.12B we have a larger point of view where we notice that strain 1 has disappeared from the population and only strain 2 remains causing the stage I_2 to oscillate together with the number of susceptible humans yet in the population, S .

We notice again in the oscillations of stage I_2 in figure 3.12B that they present many peaks in each outbreak caused again by the alterations in the entrance of new healthy mosquitoes, that in this case is not constant. From figure 3.13A we observe that the dynamics can be explained as in the case of region 1 for the seasonality case, only this time we are dealing with strain 2 instead of strain 1.

At $t = 11100$, mosquitoes are decreasing each time slower, while infected humans (in stage I_2) are increasing each time faster. By the time mosquitoes reach their lowest, infected humans reach a maximum and start to decrease (because although conditions are good, there are not enough mosquitoes). Then, the season of growing arrives for mosquitoes and there are each time more mosquitoes in the population.

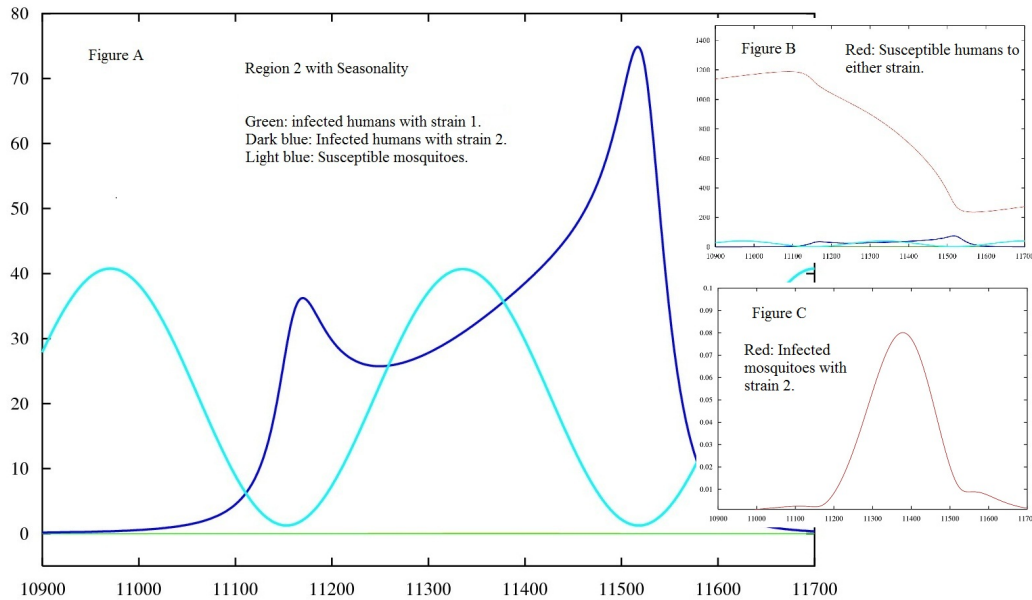


Figure 3.13: Y-axis: the number of humans. X-axis: time from 10900 (30 years) to 11700 days (32 years). Red: Human Susceptible to either strain (stage S). Dark blue: First time infected humans with strain 1 (stage I_2). Light blue: Susceptible mosquitoes to either strain (stage V_0). Figure A: Susceptible mosquitoes oscillate while the number of human infected shows a two-peaked outbreak. Figure B: Shows how the number of susceptibles decreases while the number of first time infected is increasing.

Then the infected human begin to increase again. As this happens, we observe the stage of susceptible humans (S), shown in figure 3.13B, that is decreasing as humans get infected.

3.3.5 Region III - Autonomous Case

Region III represents the case where both strains coexist being strain 1 stronger than strain 2 with $R_0 = R_0^1 > R_0^2 > 1$, $R_1 = R_0 = 2.96918$ and $R_2 = 2.57$.

Initially, all humans are susceptibles in the population, and by introducing infected mosquitoes, some with strain 1 and some with strain 2, we make the susceptible population decrease and the infected stages, I_1 and I_2 , increase. In figure 3.14 we can see this behavior and we can also notice that humans get infected faster with strain 1 than with strain 2. Also, it is strain 1 which causes more damage into the human population by infecting more humans than strain 2 because we have $R_0^1 > R_0^2 > 1$ in this region.

To understand better how each strain is affecting the population, in figure 3.15B are shown the total of infection of each strain at a given time ($I_1 + Y_1$ and $I_2 + Y_2$). The oscillations we observe occur due to the saturation of infected humans caused

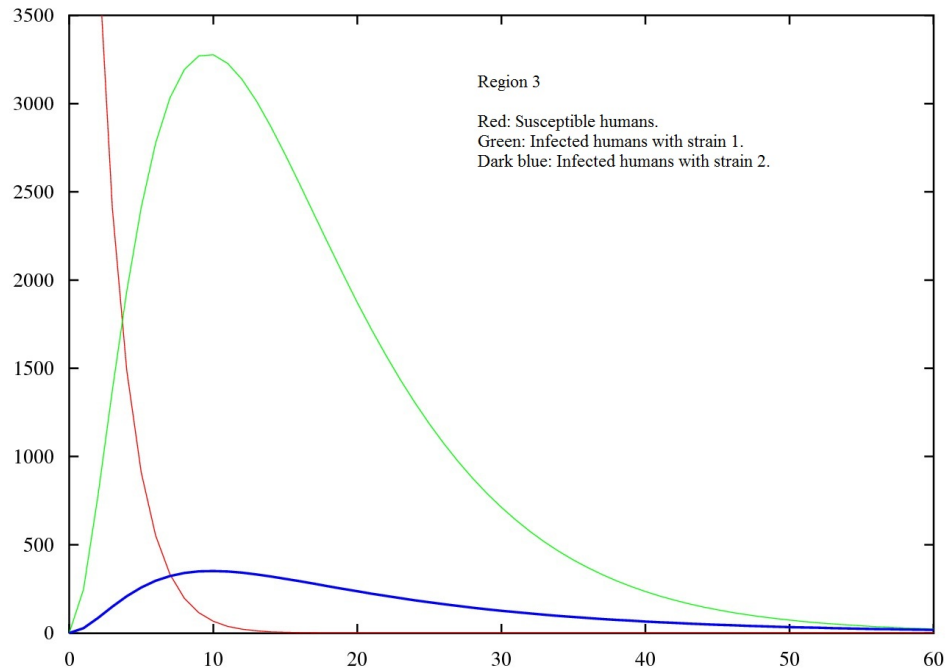


Figure 3.14: Y-axis: number of humans. X-axis: time from 0 to 60 days. The figure shows behavior of stages S , I_1 , I_2 , R for humans and V_0 for mosquitoes.

by both strains being strain 1 the stronger (and the one with more infections at the start).

Notice in the beginning of figure 3.15B that since $R_0^1 > R_0^2 > 1$, there are more humans infected with strain 1 than with strain 2. After a while strain 1 saturates the population and it has to wait till the favorable conditions reestablish again. At this moment, strain 2 has the conditions to infect the population because most humans are yet susceptible to it (but not to strain 1). Then, there comes an interval where most of the human population has already had the disease by one of the strains or maybe by both. At this moment, the disease reduces the number of infections.

In time, new humans arrive into the population of susceptibles to make it grow in number (see figure 3.15A), and the disease will be in conditions to get spread in these individuals and those who have had already one of the strains but are yet susceptible to the other. Strain 1 will infect mostly of the new arrivals causing an outbreak small than it was in the beginning, and small than the outbreak that strain 2 will cause after it. Again, this difference in magnitude of the outbreaks of both strains is due to the strength that strain 1 had at the beginning of the simulation, most of the population had already had the disease cause by strain 1 and they are now susceptible only to strain 2. So, it is normal to wait that strain 2 infects more individuals in the second outbreak than strain 1.

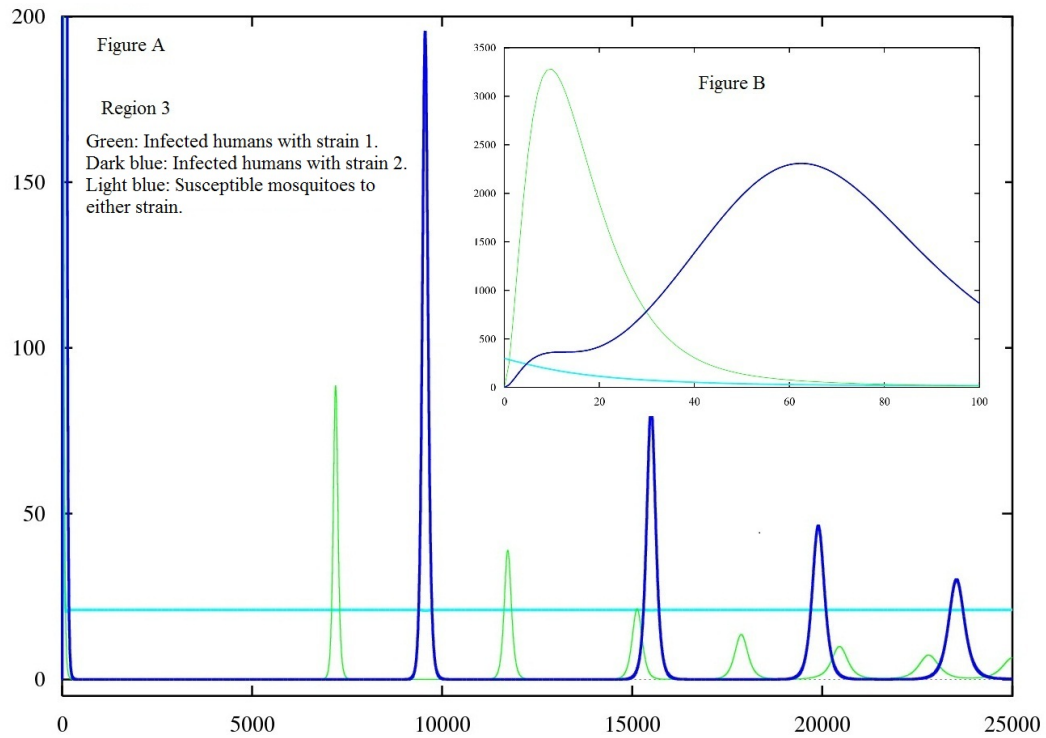


Figure 3.15: Y-axis: number of humans. Figure A: oscillations of total infections, $I_1 + Y_1$ and $X_2 + Y_2$, for each strain from day 0 to 25000 (68 years). Figure B: A detailed view of the stages in the first 100 days.

As time passes, the situation is more difficult for strain 1 than for strain 2, and though both are decreasing, strain 1 decreases faster than strain 2.

Oscillations in these stages, $I_1 + Y_1$ and $I_2 + Y_2$, are due to the movement of individuals from stage I_1 to Y_2 and from stage I_2 to Y_1 and the entrance of new susceptibles.

Oscillations for strain 1 are more frequent than oscillations for strain 2, but they are weaker in the case of strain 1. This is caused by the election of values for the parameters assign to each strain (see table 3.3).

3.3.6 Region III - Seasonality Case

Region III represents the case where both strains coexist being strain 1 stronger than strain 2 with $R_0 = R_0^1 > R_0^2 > 1$, $R_1 = R_0 = 2.96918$ and $R_2 = 2.57$. In the seasonality case new mosquitoes arrive to the susceptible stage (V_0) at a variable

rate $q(t) = 1 + \cos(2\pi t/365)$ which depends on time. The first simulation for the seasonality case is presented next with the figure 3.16A where the first 70 days are shown.

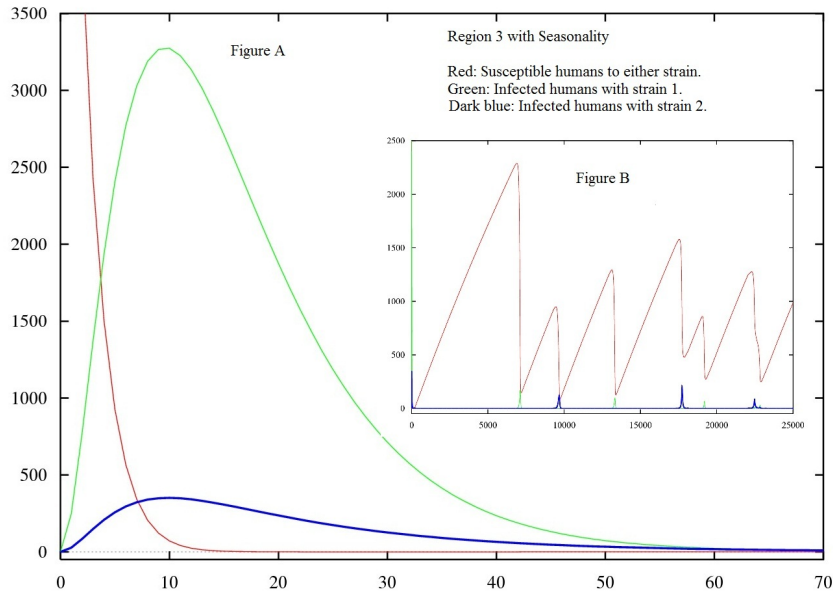


Figure 3.16: Y-axis: the number of humans. X-axis: time from 0 to 70 days. Red: Human Susceptible to either strain (stage S). Green: First time infected humans with strain 1 (stage I_1). Dark blue: First time infected humans with strain 2 (stage I_2). Figure A: Susceptible mosquitoes decrease while the number of infected humans increases, both strains. Figure B: Shows a wider look of the oscillations of S , I_1 and I_2 .

It is shown on 3.16A we can see that both strains coexist on the first 70 days. In figure 3.16B we can see that both strain continue to be in the population and that they both oscillate. In figure 3.17 the outbreaks produced by strain 1 are more frequent than those produced by strain 2. In the same figure the outbreaks for strain 2 seems to be infecting sometimes more humans and sometimes less. When continuing the simulation we noticed that the number of infected by strain 2 is at the end decreasing (figure 3.18).

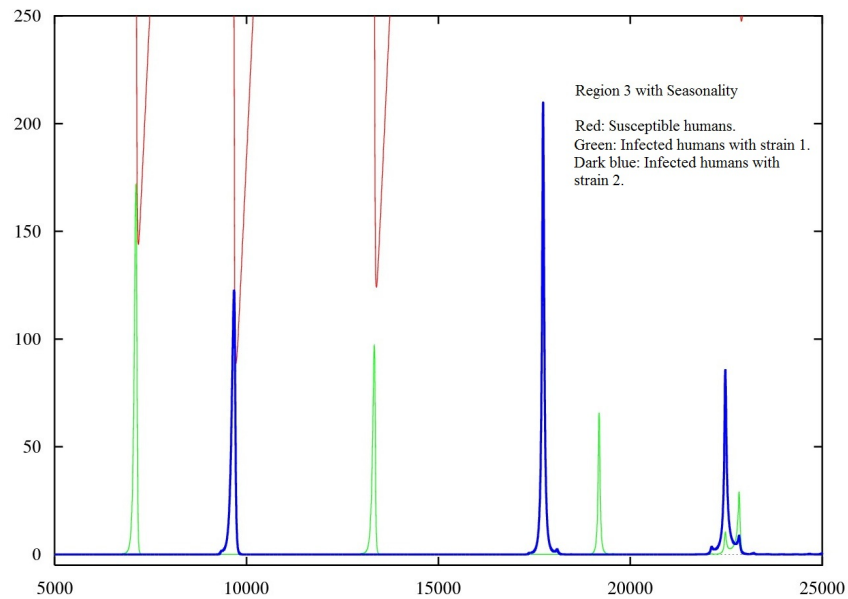


Figure 3.17: Y-axis: the number of humans. X-axis: time from 5000 (13 years) to 25000 days (68 years). Red: Human Susceptible to either strain (stage S). Green: First time infected humans with strain 1 (stage I_1). Dark blue: First time infected humans with strain 2 (stage I_2). Both strains coexist at all time shown in the simulation, and stages I_1 and I_2 oscillate.

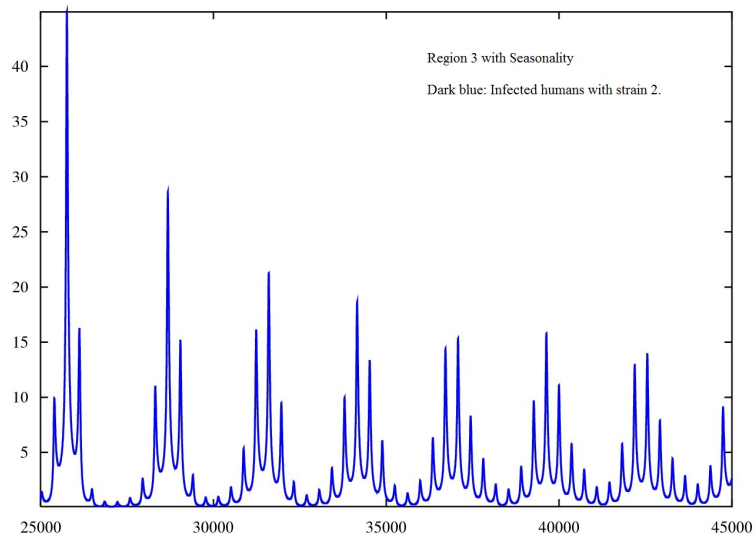


Figure 3.18: Y-axis: the number of humans. X-axis: time from 25000 (68 years) to 45000 days (123 years). Dark blue: First time infected humans with strain 2 (stage I_2). Figure shows the oscillation of I_2 is slowly decreasing.

Figure 3.19 allows a closer view of oscillations of stages I_1 and I_2 due to the oscillation of V_0 . At time $t = 22100$, I_2 starts to increase, but since V_0 is being reduced, there are less mosquitoes to infect in the population, so infection by strain

1 is momentarily stopped. Later, the number of susceptible mosquitoes increase and there is room for the infection to spread through the human population. We observe that at time $t = 22500$ we have the maximal for stages I_1 and I_2 , and it is observed to happen after the minimal for the population of susceptible mosquitoes. This is because the disease has infected most of mosquitoes and they spread the disease into the human population. Strain 2 is the one with the highest number of infected humans due to the cross immunity of the disease. Once the infected mosquitoes die and new mosquitoes enter in the population, number of individuals at stages I_1 and I_2 start to decrease.

After time $t = 22900$, there is an outbreak again, this time strain 1 infects more individuals than strain 2, nevertheless it is less than half than it was the previous outbreak of strain 1. Since that in this case we have $R_0^1 > R_0^3$, this implies that strain 1 is stronger although it is not seeing yet in the simulations. When we continue the simulation to see what happens with strain 1 we noticed that it presents the same type of oscillations as we discuss for strain 2, only it goes slower, that means the disease strain 1 will remain longer in the population before disappearing.

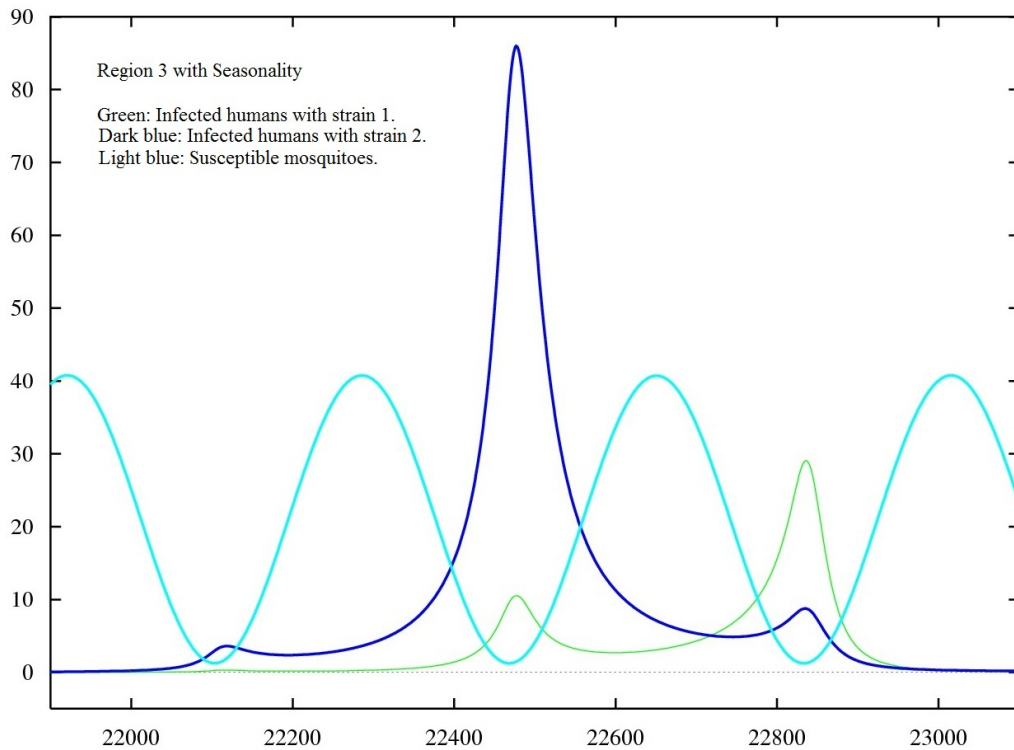


Figure 3.19: Y-axis: the number of humans. X-axis: time from 21900 (60 years) to 24000 days (65 years). Green: First time infected humans with strain 1 (stage I_1). Dark blue: First time infected humans with strain 2 (stage I_2). Light blue: Susceptible mosquitoes to either strain (stage V_0). The oscillation of stages I_1 and I_2 is due to the oscillation of V_0 .

3.3.7 Region IV - Autonomous Case

Region IV represents another case where both strains coexist but strain 2 is stronger than strain 1. For this case, $1 < R_0^1 < R_0^2 = R_0$, $R_1 = 2.71$, $R_2 = R_0 = 3.5$.

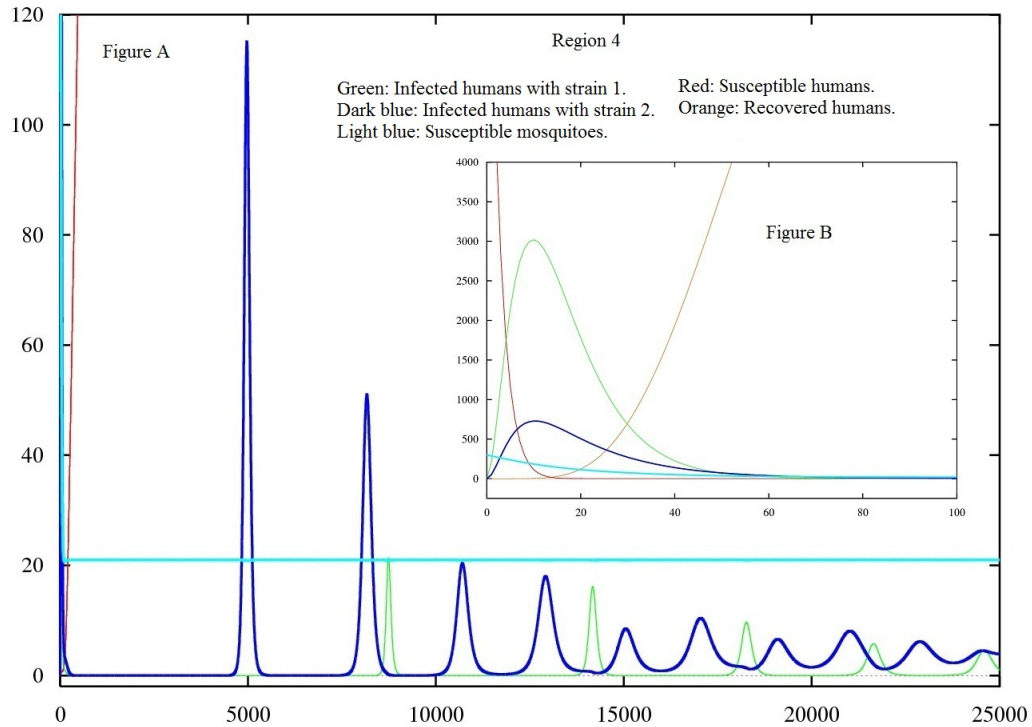


Figure 3.20: Y-axis: number of humans. Figure A: shows oscillations of I_1 and I_2 from day 0 to 25000 (68 years). Figure B: Shows stages S , I_1 , I_2 , R , for humans and V_0 for mosquitoes from day 0 to 60.

As in region III, initially, all humans are susceptibles in the population, and by introducing infected mosquitoes, some with strain 1 and some with strain 2, we make the susceptible population decrease and the infected stages, I_1 and I_2 , increase. In figure 3.20B we can see this behavior and we can also notice that humans get infected faster with strain 2 than with strain 1.

Although we have chosen different values of parameters for strain 1 than for strain 2, we observe a very similar behavior in region IV than the one we observed in region III. In region IV we observe that oscillations for strain 2 are more frequent than for strain 1, but this time strain 1 gets reduced faster.

3.3.8 Region IV - Seasonality Case

Region IV represents another case where both strains coexist but strain 2 is stronger than strain 1 with $1 < R_0^1 < R_0^2 = R_0$, $R_1 = 2.71$, $R_2 = R_0 = 3.5$. In the seasonality case, the new susceptible mosquitoes enter the population at a variable rate $q(t) = 1 + \cos(2\pi t/365)$ which depends on time t .

The figure 3.21A shows how is the dynamic of the stages S , I_1 , I_2 , of the disease in a lapse of 80 days in the beginning of the simulation.

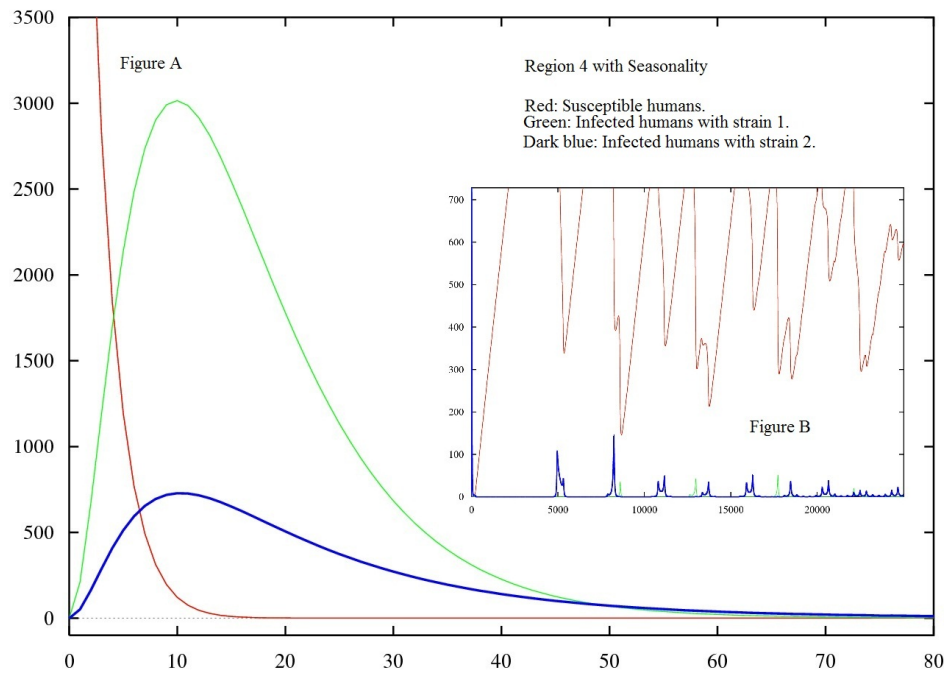


Figure 3.21: Y-axis: the number of humans. X-axis: time from 0 to 80 days. Red: Human Susceptible to either strain (stage S). Green: First time infected humans with strain 1 (stage I_1). Dark blue: First time infected humans with strain 2 (stage I_2). Figure A: Susceptible mosquitoes decrease while the number of human infected increase. Both strains coexist in the population. Figure B: Shows how the number of susceptibles oscillates while the number of first time infected humans for each strain also oscillates.

Figure 3.22 shows that both strains continue to exist in the population and oscillate. Strain 2 presents outbreaks more frequently than strain 1. When continued, the simulation shows that both strains are slowly decreasing and strain 2 stays longer in the population than strain 1.

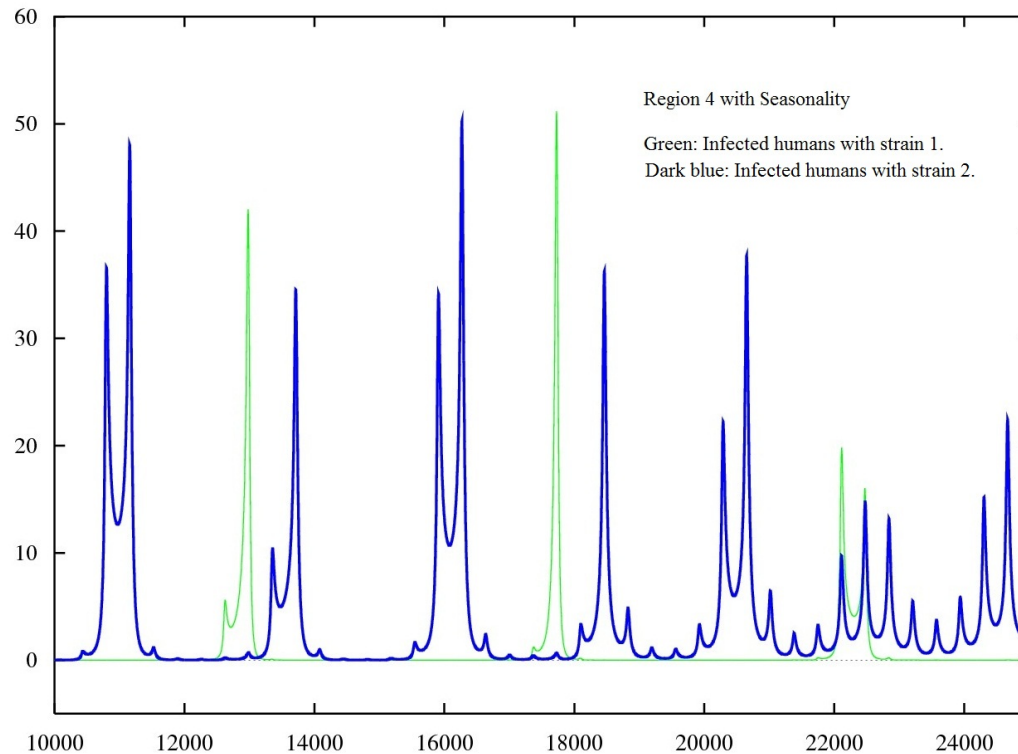


Figure 3.22: Y-axis: the number of humans. X-axis: time from 10000 (27 years) to 25000 days (33 years). Green: First time infected humans with strain 1 (stage I_1). Dark blue: First time infected humans with strain 2 (stage I_2). The oscillations of each strain seems to be irregular. Outbreaks for strain 2 are more frequent than those for strain 1.

3.3.9 Observations

Although we could have expected differently, there were oscillations presented in the autonomous model, which implies that the disease "comes and goes" and comes back again. This is actually always observed in the behavior of Dengue dynamics in real life. What is more remarkable is the fact that this happens even without introducing the effects of seasonality in the model though, in any case, the disease finally extinguishes.

Considering the effects we observed from the curves with forced annual periodicity, we can see that they cause more damage, in terms of the amount of people that gets infected, and this happens especially when its annual seasonal periodicity (taking $q(t) = 1 + \cos(2\pi t/365)$).

Chapter 4

Wavelets

We will make use of Wavelet Transform (WT) as a tool with the objective of validate the effectiveness and confidence of the model (1.3) and also to see if it is good to describe and analyze real cases. In this chapter we will introduce the WT by giving a brief introduction to wavelet theory and we will make clear which type of wavelet we will be using in a later section. We show the basic concepts of wavelets, continue wavelets and discrete wavelets, and how a wavelet is done. Later, we give the definitions of cross wavelet transform (XWT) and wavelet transform coherence (WTC) which will help us to compare the observations obtained from real data with the solutions of the model (1.3).

4.1 An Introduction to Wavelets

For years scientists have applied mathematical transformations to signals to obtain further information from them that cannot be read in the raw signal. A raw signal is the one obtained in time domain, while the processed signal is obtained from the application of a mathematical transformation into a signal, i.e., a processed signal is a transformed signal [43].

There are many mathematical transformations in use. Examples of these are: Hilbert transformation, Wigner transformation, Radon transformation, short-time Fourier transformation, Fourier transformation and Wavelet transformation. The most famous transform is Fourier, proposed by Joseph Fourier in early 1800's, where the idea of approximation is done using superposition of functions sine and cosine. When applied we obtain a Frequency Spectrum and, with this, the Fourier transformation tell us what frequencies exist in the signal. So, if the purpose is finding the frequency content of a signal then we use Fourier Transform (FT) [20].

However, FT is not a convenient technique for this study since we are dealing with a problem where frequency varies with time, which produces a non-stationary signal. By applying FT we would only obtain the information of what spectral frequency components exist but we will not be able to know when. This is why FT is not of use with biological signals, since they all are non-stationary and we are interested in knowing not only which frequencies are involved, but also at what time

they appear [9, 43].

We need to know when in time the spectral components are located, to do that we need a transform that can give us a time-frequency representation of the signal. This could be done using the Windowed Fourier transform (WFT), the wavelet transform (WT), and others, too. While using WFT we can get to know all the frequency components involved in the signal and the time where they are located. But there is an important reason why we do not choose WFT to study the model (1.3) and it has to do with the resolution problem. The resolution problem consist in the fact that we can only know the time intervals in which certain band of frequencies exist.

With FT there is no resolution problem in frequency domain because we know exactly what frequencies exist in the signal, and we know the exact value of the signal at every instant of time. In the case of WFT the signal is divided into small enough segments where the signal can be assumed to be stationary. The width of these segments or windows is known as the support of the window. In WFT, the window is of finite length and it only covers a portion of the signal, therefore we get a poor frequency resolution, we do not know what exact frequencies appear but we know only a band of frequencies that exist in an interval of time. To obtain the stationarity we must have a short enough window in which the signal is stationary. The narrower we make the window, the better the time resolution but poorer frequency resolution. On the contrary, if we take a wider window we can get better frequency resolution but poor time resolution.

For this study we have chosen the Wavelet Transform since it has variable resolution in advantage to WFT which has fixed resolution. The resolution indicates what spectral components exist at any given interval of time. The problem with the WFT is the width of the window function that is used which is fixed from the beginning and that does not allow us to get good resolution.

Using wavelets we can vary the width and that permit us to obtain quality information from the signal. With the wavelet transform (WT) higher frequencies are better resolved in time and lower frequencies are better resolved in frequency. Thus we have that a high frequency component can be better located in an interval of time than a low frequency component [43].

The Continuous Wavelet Transform (CWT) uses an alternative approach to overcome the resolution problem: the Multi Resolution Analysis (MRA). The MRA analyzes different frequencies with different time resolutions. The procedure to wavelet analysis is to choose a wavelet prototype function (called mother wavelet). Then we procede to calculate the CWT for all values of the scale s .

There are many types of mother wavelet, such as Meyer, Morlet, Mexican hat,

Daubechies, Haar, to mention some. Wavelets can be separated in discrete and continuous, and also among the continuous there are real-valued and complex-valued wavelets [20]. For this study we have chosen the Morlet wavelet, which is a complex-valued one.

Some important definitions and information that we will use in this chapter and we should have in mind are given. The translation is related to the location of the window as it is shifted through the signal. The scale is defined as $1/\text{frequency}$. High scales correspond to non-detailed global view of the signal, low scales correspond to a detailed view. Scaling, as a mathematical operation, either dilates or compresses a signal. Larger scales correspond to dilated signals. Small scales correspond to compressed signals. Low frequencies correspond to a global information of a signal, whereas high frequencies correspond to a detailed information of a hidden pattern in the signal period.

The CWT is a powerful mathematical instrument that transforms a time series to a time-scale domain [34]. The procedure to transform a signal into a wavelet in the time frequency space is:

Once the mother wavelet has been selected computation starts with a fixed value of the scale s and the CWT is computed for all values of s , smaller and greater than the starting value. As scale increases, wavelet will dilate. The wavelet is placed at the beginning of the signal corresponding with time $t = 0$. The wavelet function at each value for the scale is multiplied by the signal and then integrated over all times. The result of the integration is multiplied then by the constant number $\frac{1}{\sqrt{s}}$ (to normalize the process so that the transformed signal will have the same energy at every scale. The result is the value of the CWT at time $t = 0$, $s = 1$ in the time-scale plane. Then the wavelet at scale 1 is shift to the right by τ units to time $t = \tau$ and we compute to get the transform value at $t = \tau$, $s = 1$ in the time-frequency plane. This process is repeated until the wavelet reaches the end of the signal. Then one row of points on time-scale plane for the scale $s = 1$ is now completed. Then s is increased by a small value and all the procedure is repeated for every value of s . When the process is completed for all desired values of s , the CWT of the signal has been calculated.

Before starting the analysis we considered presenting some basic definitions on wavelets and the selected Morlet wavelet.

To be called a wavelet, the analyzing function should be admissible, which means the average of the integrable function should be zero [15], this is called the "admissibility condition". The "similarity condition" which is another requirement to have a wavelet is that the scale decomposition should be obtained by the translation and dilation of only one "mother function" [15]. And finally, there should be one reconstruction formula to recover the original signal from its wavelet coefficients, this is the invertibility condition and it is due to that the inverse wavelet transform can

exist.

The Morlet wavelet is an example of a function with zero mean which satisfies all the conditions and that can be localized in both time and frequency space [47]. Assuming that we have a time series, x_n , with equal time spacing δt and $n = 1, \dots, N - 1$. Also, consider $\psi_0(\eta)$, that depends on a nondimensional "time" parameter η . Wavelets are defined as

$$\psi_{s,\eta}(t) = \frac{1}{\sqrt{s}} \psi\left(\frac{t - \eta}{s}\right)$$

The Morlet wavelet consist of a plane wave modulated by a Gaussian:

$$\psi_0(\eta) = \pi^{-1/4} e^{i\omega_0\eta} e^{-\eta^2/2}$$

where ω_0 is the non-dimensional frequency, taken to be 6 to satisfy the admissibility condition [47].

The wavelet transform of a time series x_n with respect to a chosen mother wavelet is performed as follows:

$$W_n(s, \eta) = \frac{1}{\sqrt{s}} \int_{-\infty}^{\infty} x(t) \psi^*\left(\frac{t - \eta}{s}\right) dt$$

where the asterisk denotes the complex conjugate form [5].

The wavelet coefficient $W_n(s, \eta)$ represents the contribution of the scale s to the signal when time is at different position η . The computation of the wavelet transform is done along the signal $x(t)$ by increasing the parameter η over a range of scales s until all coherent structures within the signal can be identified.

The continuous Wavelet Transform of a discrete sequence x_n is defined as the convolution of x_n with a scaled and translated version of $\psi_0(\eta)$:

$$W_n(s) = \sum_{n'=0}^{N-1} x_{n'} \psi^*\left[\frac{(n' - n) \delta t}{s}\right]$$

where ψ^* denotes the complex conjugate [47].

When we vary the wavelet scale s and translate it along the localized time index n , we can construct a picture showing both the amplitude of any features versus the scale and how this amplitude varies with time.

Since the wavelet function $\psi(\eta)$ is complex, its wavelet transform $W_n(s)$ is also complex and can be divide into real part (amplitude) and imaginary part (phase). We define the Wavelet Power as $|W_n(s)|^2$ [47]. And the complex argument of $W_n(s)$ can be interpreted as the local phase [21].

Errors in the transformation will occur at the beginning and end of the Wavelet Power Spectrum because we are dealing with a finite-length time series. One way to reduce the error is to pad the end of the time series with zeroes before doing the Wavelet Transform and then remove them afterward. Thus, the cone of influence (COI) is formed.

The COI (which appears in the wavelet as a blurry region) is where edge effects become important [47]. The cone of influence helps us to identify the region of the wavelet where we can trust in the information from that part which is not completely reliable due to the fact that at the beginning and end of the wavelet, at the moment of doing the convolution, there are parts where the signal is not enough big for the Morlet to cover it. So the program will fill "emptiness of the signal" with zeros just to be able to calculate the convolution. In this study we took the COI area in which the wavelet power caused by a discontinuity at the edge has dropped to e^{-2} of the value at the edge [21].

It is assumed that the time series has a mean power spectrum; if a peak in the Wavelet Power Spectrum is significantly above this background spectrum, then it can be assumed to be a true feature with a certain percent confidence. As a definition, "significant at the 5% level" is equivalent to "the 95% confidence level", and implies a test against a certain background level. While the "95% confidence interval" refers to the range of confidence about a given value [47]. The confidence interval is defined as the probability that the true wavelet power at a certain time and scale lies within a certain interval about the estimated wavelet power [47].

When comparing two signals, the Cross Wavelet Transform (XWT) is useful as it finds regions in time frequency space where both time series show high power at same time. The Cross Spectrum Denotes the co-varying power of two processes, that is, the predictive information between each other. Sometimes, a superimposed independent variance only appears in the single spectra but not in the cross spectra; this also implies that the cross spectrum vanishes for two independent processes [34].

Given two time series X and Y, with wavelet transforms $W_n^X(s)$ and $W_n^Y(s)$, we can define the Cross-Wavelet Spectrum as

$$W_n^{XY}(s) = W_n^X(s) W_n^Y(s)$$

The cross-wavelet Spectrum is a complex number [47], and therefore we can define the Cross-Wavelet Power as the argument of a complex number, that is

$$|W_n^{XY}(s)|$$

The complex argument of $W_n^{XY}(s)$ can be interpreted as the local relative phase between X and Y in time frequency space [21]. The relative phase relationship is shown as arrows in the XWT with in-phase pointing right, anti-phase pointing left [21].

Another tool at hand to compare signals with wavelet analysis is the Wavelet Transform Coherence (WTC) which is defined as the square of the Cross-Spectrum normalized by the individual power spectra. This gives a quantity between zero and one, and measures the Cross-Correlation between two time series as a function of frequency [47]. The Wavelet Coherence (WTC) finds regions in time frequency space where the two time series co-vary (but does not necessarily have high power). The coherence (or coherency) is defined as the modulus of the cross spectrum, normalized to the single spectra. Exhibiting values between zero and one, it quantifies the linear relationship between two processes. In general, one rarely finds perfect linear dependence [34].

We can define the WTC of two series as

$$W_n^2 = \frac{|W_n^{XY}|^2}{|W_n^X|^2 |W_n^Y|^2}$$

Notice that this definition is very similar to that of the traditional correlation coefficient. It can be useful to think of the WTC as the localized correlation coefficient in time frequency space [21].

In this chapter we will show how we have used wavelets as a tool to help us compare data from simulations of the model (1.3) with data from real databases. To get data from the model we used XPPAUT and we run simulations for the model using parameters in an established region (see chapter 3, table 3.4). We have counted the number of infected humans, sometimes we made a count by days and in other case we count them by weeks (depending on the database we have to be compared with the data from the solution of the model).

We obtained files describing information (like date of begin of the disease, gender, age, location, etc.) of people who had Dengue disease in Mexico during 2002 to 2009. We got data from the city of Cuernavaca which tells us how many people were sick with Dengue day by day from 2008 to 2009.

Also we made use of data from four Mexican states (Oaxaca, Chiapas, Guerrero and Veracruz); for this case we added the total of infected people in those four states each week from 2002 to 2009.

Finally, we made use of the online report of Google Trends in Dengue for Mexico (from January 12th, 2003, till September 8th, 2012). Google Trends consists of the statistics that shows how often a particular search-term is entered relative to the total search-volume across various regions of the world, and in various languages, in this case we search for "Dengue" trends in Mexico.

4.2 Analysis of the Model Using Wavelets

We have found the solutions of the model to obtain data and we have applied the Morlet wavelet approximation to it using Matlab tools specially created for wavelet analysis and Grinsted-Moore-Jevrejeva's code ([21]).

Since in Mexico only one strain dominates each year, we found more appropriate to begin the study with Region I, where only strain 1 survives in the population. To explain what we will see in the subsequent figures, we will start with the Continuous Wavelet Transform (CWT) of the data from the model (1.3) in Region I. The data of the model was obtained by solving the model (1.3) from time 0 to 15000 although we only display data from time 5000 to 15000 days. In the bottom of figure 4.1 we show the histogram done with the sum $I_1 + I_2 + Y_1 + Y_2$ of all infected humans at each instant of time t and we call this the time series. This graph will be referred to as the time series of the data that will be used to construct the CWT. The CWT corresponding to the data of the Model (1.3) Region I for the autonomous case is shown up in figure 4.1 with its time series below.

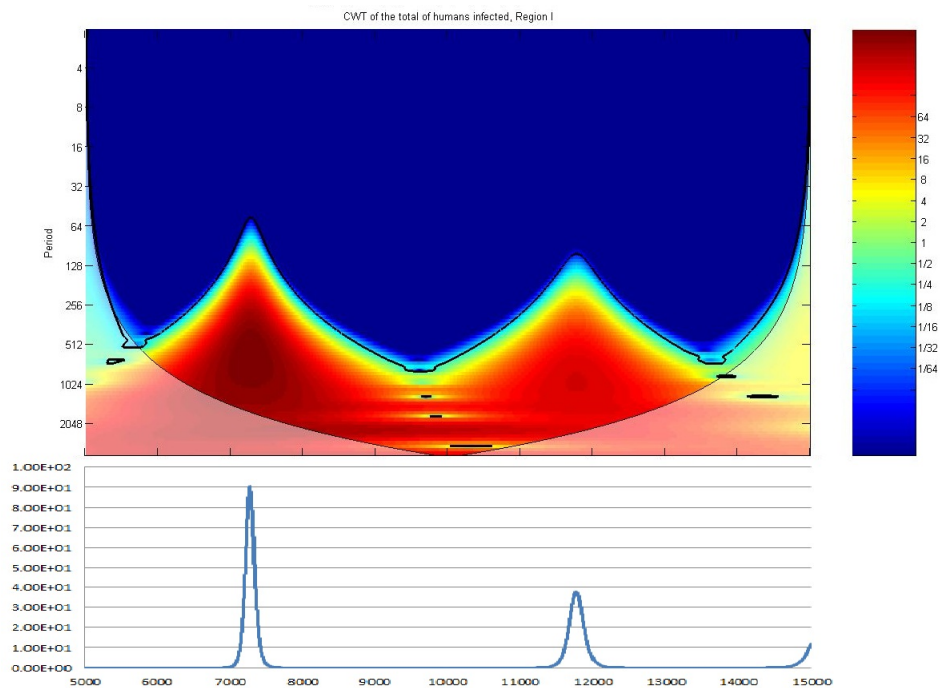


Figure 4.1: Top: Continuous Wavelet Transform of data generated with the model (1.3) using Region I. The vertical left axis indicates period (in days). The horizontal axis indicates time (in days). The vertical right axis is the color scale used to get a better distinction between the different contributions which appear in the CWT where red is higher and blue is less. Bottom: Time Series involving 10000 days for the autonomous model in Region I. On the vertical-axis we have the number of infected humans that are in the population (the sum $I_1 + I_2 + Y_1 + Y_2$) at each time (horizontal-axis in days). The vertical axis indicates the proportion of infected humans in the population at the time given in weeks in the horizontal axis.

In the top of figure 4.1 we show the corresponding CWT of data from the model (1.3) using parameters in region I (see table 3.4 in chapter 3). The CWT expands the time series into time-frequency space or, as in this case, time-period. The vertical left axis represents the period (in days) while the horizontal axis shows time (in days). To the right there is the color scale used to show the power of the wavelet at an specific period and time. The red color implies a higher wavelet power and blue the lowest. In the wavelet graph there is a blurry region below on either end indicating the "cone of influence". The thick black contour designates the 5% significance level against red noise.

We can see the signal shows high power larger than 64 as it is shown in the color scale to the right, and this occurs at times between 6500 and 7600 days coinciding with the first outbreak shown in the time series.

The power is less than $1/64$ for periods below 64 at all times for the signal in the CWT. This tells us that the signal presents no variations in scales of time of less than 64 days. This tells us that when working with Dengue it takes more than 64 days for us to be able to observe where is the disease leading to, if it is growing to an outbreak or if it is being reduce to disappear or equilibrate itself.

In the subsequent sections we present the comparison of the solution of the model (1.3) with three real cases. The comparison is done through the use of the Cross Wavelet Transform (XWT) and also the with Wavelet Transform Coherence (WTC) of the signal obtained with the model (1.3) in different regions and the signal in each case.

4.3 Comparison with Four Mexican States data

In this section we present an analysis of real data series using Continuous Wavelet Transform (CWT). We analyzed real data obtained from four mexican states (Chiapas, Guerrero, Oaxaca and Veracruz) which is organized by weeks and includes 416 values of data.

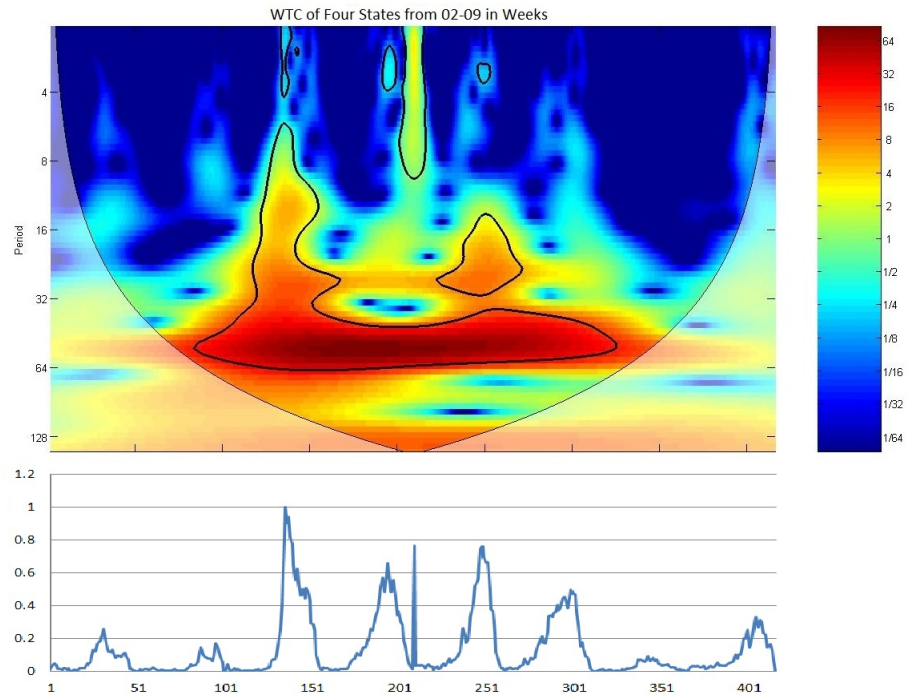


Figure 4.2: Top: Continuous wavelet transform of a real data basis from four Mexican states. The vertical left axis indicates period (in weeks). The horizontal axis indicates time (in weeks). The vertical right axis is the color scale used to get a better distinction between the different contributions which appear in the CWT where red is higher and blue is less. Bottom: its Time Series. The vertical axis indicates the proportion of infected humans in the population at the time given in weeks in the horizontal axis.

We can notice in the time series of figure 4.2 that there are more number of cases around the 135th week since the beginning of the list and from there oscillates with an amplitude which seems to be decreasing. With this data we obtained the continuous wavelet transform shown above in the figure 4.2. We can see that power is concentrated mainly among the 90 to 325 weeks. This coincides also with what we see in the time series below for it is at the same interval from week 0 to 325 that there are more infected people.

The thick contours enclose regions of greater than 95% confidence (for a red-noise process) and the cone of influence (COI) where edge effects might distort the picture is shown as a lighter shade. The L-shaped contour encloses a region between periods 6 to 64, but the higher power appears near period 64, meaning that the signal has variations in scales of time of near 64 weeks. The power near period 64 weeks is 64 as shown in the color bar.

Another smaller contour appears in figure 4.2 between weeks 221 and 261 among period 16 to 32 but with a weak power of 4.

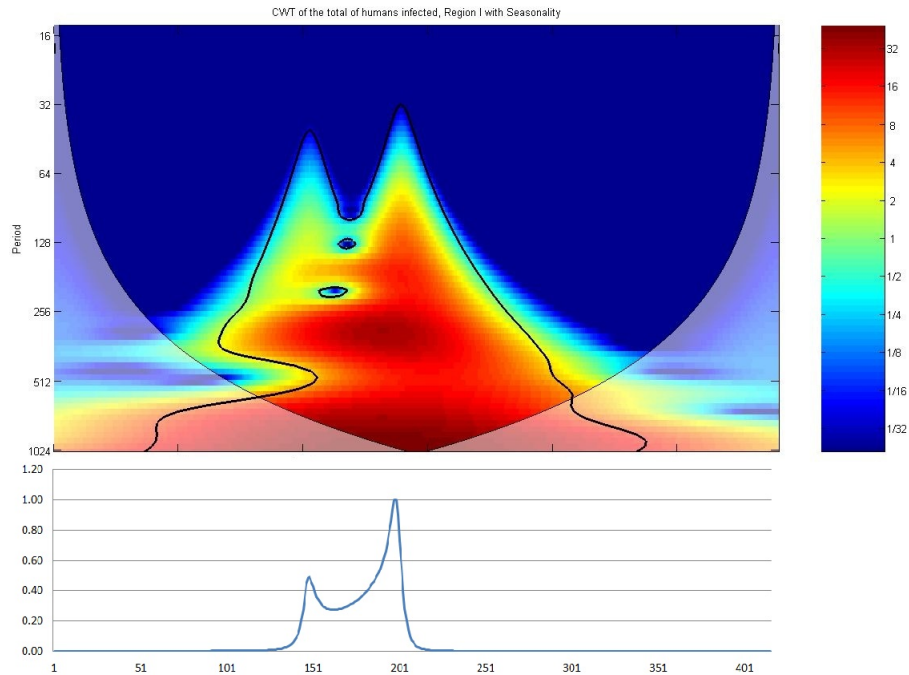


Figure 4.3: Top: Continuous wavelet transforms for the model (1.3) Region I with Seasonality. The vertical left axis indicates period (in weeks). The horizontal axis indicates time (in weeks). The vertical right axis is the color scale used to get a better distinction between the different contributions which appear in the CWT where red is higher and blue is less. Bottom: its Time Series. The vertical axis indicates the number of infected at the time given in weeks in the horizontal axis.

We want to compare this data with data obtained from the model. To do this comparison we have selected the region I with Seasonality for two reasons. First of all, because in Mexican States one strain dominates the disease, and this is the case for Region I and II, we selected Region I. And the second, we chose seasonality because this way we simulate the variations of the amount of mosquitoes during a year. In order to compare we must have same size (number of data) and same interval length (daily, weekly, etc.) that is why we selected data from the model from day 10500 to 13405. The CWT and time series obtained from the model (1.3) are shown in figure 4.3.

We observe in figure 4.3 that the black contour encloses a big part of the CWT for an interval of time from week 61 to 340. From a period of 64 and up the power is higher than 8. But the most significant power appears close to period 256 since here the scale of color indicates 32. The same phenomena happens again near period 512 where the scale of color indicates again 32.

We want to know if there are similarities between both CWT so we compared them. In figure 4.4 we show both CWT: the one for the four states (on top) and the one for the model with seasonality (1.3) in region I (bottom).

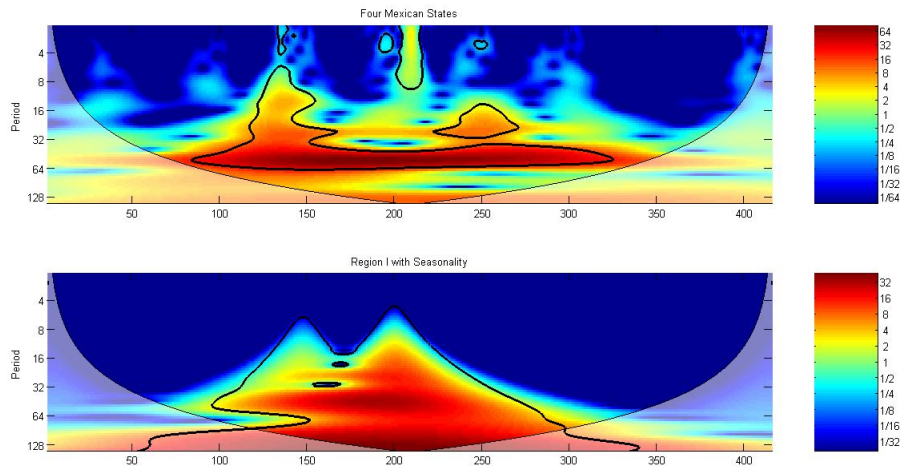


Figure 4.4: Display of both continuous wavelet transforms for Four States data (top) and the model (1.3) Region I with Seasonality (bottom).

In figure 4.4 we show the Continuous wavelet transform from both data series. We can see that both CWT have high power in the 32 to 64 week band around the 100 week and it is above the 5% level of significance. We proceed to show the Cross Wavelet Transform which helps us see if there are similarities in the powers for both series.

The Cross Wavelet Transform (XWT) in figure 4.5 shows that the common features we mentioned previously from the individual wavelet transforms stand out as being significant at the 5% level (95% confidence level) from 100-300 week, meaning that the signals are very similar between the 100 to 300 week.

In the XWT, the relative phase relationship is shown as arrows with in-phase pointing right, and anti-phase pointing left. In figure 4.5 with the arrows pointing in many directions, the XWT does not give us much information. There is a line of arrows pointing right between period 32 and 64 but it is not enough for us to conclude that there is a linear relationship between both signals.

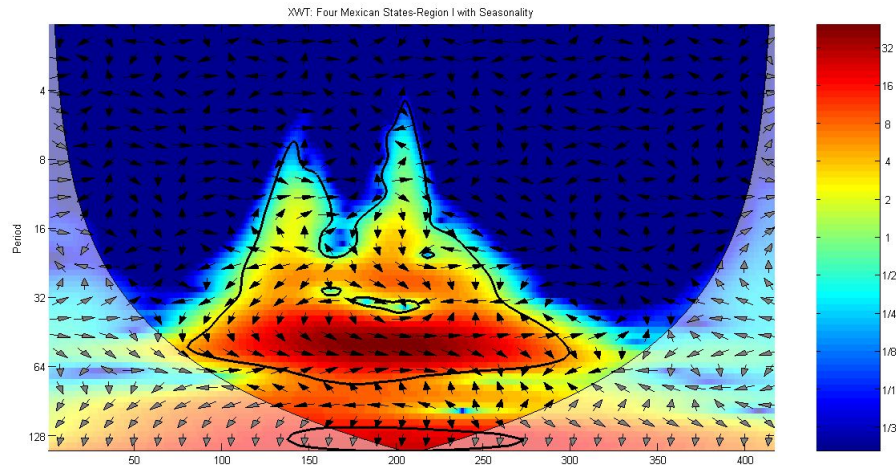


Figure 4.5: Cross Wavelet Transform of the model (1.3) Region I compared with the Four States data. The relative phase relationship is shown as arrows (with in-phase pointing right, anti-phase pointing left).

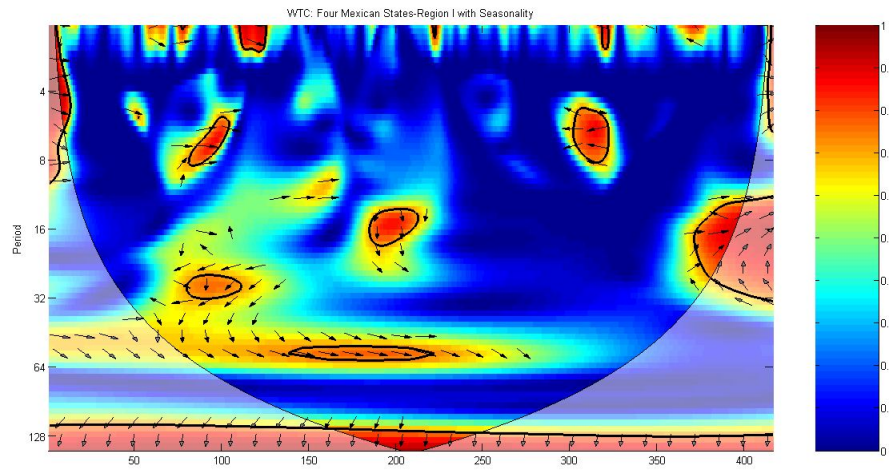


Figure 4.6: Wavelet Transform Coherence. The thick contours show the 5% significance level against red noise.

Cross wavelet power reveals areas with high common power, but another useful measure is how coherent the cross wavelet transform is in time frequency space [21]. We present the Coherence for both series in figure 4.6.

In the Coherence shown in figure 4.6 we can notice several sections in red, but they are very small. We do not find any correlation in the two signals from real data and the model.

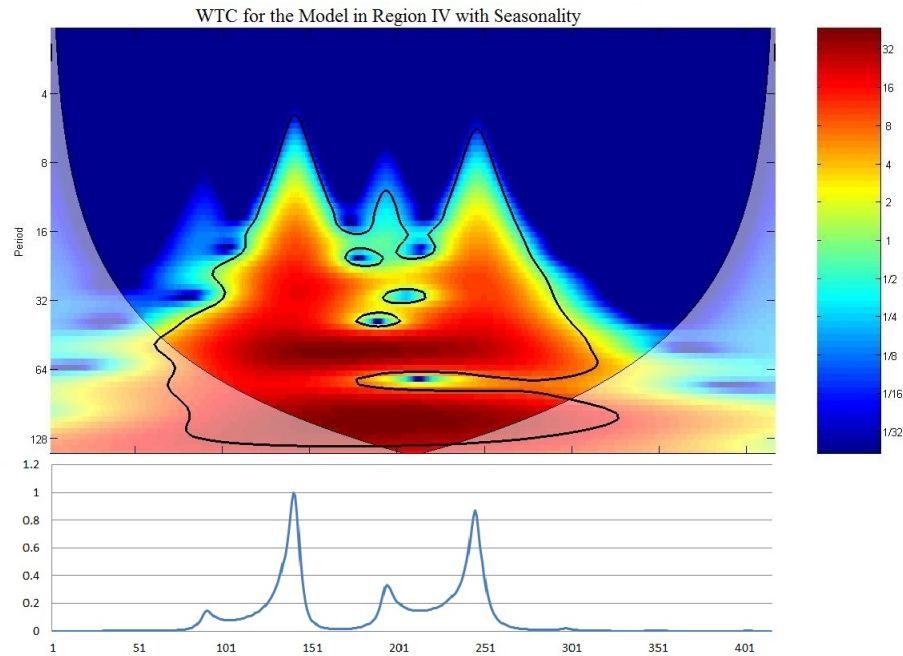


Figure 4.7: Top: Continuous wavelet transforms for the model (1.3) Region IV with Seasonality. The vertical left axis indicates period (in weeks). The horizontal axis indicates time (in weeks). The vertical right axis is the color scale used to get a better distinction between the different contributions which appear in the CWT where red is higher and blue is less. Bottom: its Time Series. The vertical axis indicates the number of infected at the time given in weeks in the horizontal axis.

For the same data we compared again with data from the model in another Region. To do this comparison we have selected the region IV, where both strains coexist, with seasonality because this way we simulate the oscillations of the amount of mosquitoes during a year. In order to compare we set again same size (number of data) and same interval length (daily, weekly, etc.) of data and we selected data from the model from day 12005 to 14910. The CWT and time series obtained from the model (1.3) are shown in figure 4.7.

We observe in figure 4.7 that the black contour encloses a big part of the CWT for an interval of time from week 61 to 311. From a period of 16 and up the power is higher than 8. But the most significant power appears close to period 64 since here the scale of color indicates 32. The same phenomena happens again near period 128 where the scale of color indicates again 32.

We want to know if there are similarities between both CWT so we compared them. In figure 4.8 we show both CWT from the model with Forced Periodicity 1.3 in region I (on top) and the one for the four states (below).

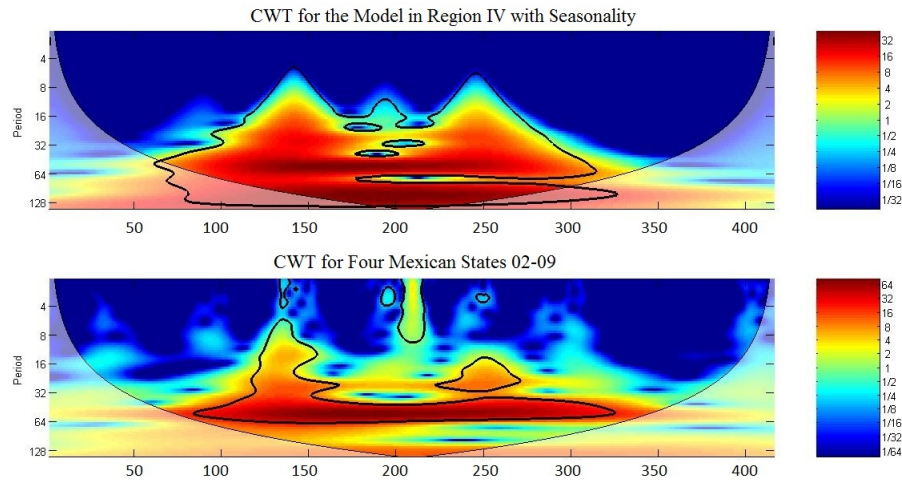


Figure 4.8: Display of both continuous wavelet transforms for (top) the model (1.3) Region IV with Seasonality and (bottom) Four States data.

In figure 4.8 we show the Continuous wavelet transform from both data series. We can see that both CWT have high power in the 32 to 64 week band around the 100 week and it is significant at the 5% level (95% confidence level). We continued the experiment and we proceeded to get the Cross Wavelet Transform to help us see if there are similarities in the powers for both series.

The Cross Wavelet Transform in figure 4.9 shows that the common features we mentioned previously from the individual wavelet transforms stand out as being significant at the 5% level (95% confidence level) from 80-280 week, meaning that the signals are very similar in that interval. There are arrows pointing mostly to the right inside the region of interest, so we may conclude that there is a linear relationship between both signals.

Cross wavelet power reveals areas with high common power, but another useful measure is how coherent the cross wavelet transform is in time frequency space [21]. We present the Coherence for both series in figure 4.10.

In the Coherence shown in figure 4.10 we can notice several sections in red, but one main involves a big part of the image and contains a darker region inside from week 75 to 250 around the 24th to 64th period, with the arrows pointing right implying that there is co-variance of data in this region. According to Grinsted et al. [21], although it is possible for two signals to be perfectly correlated at one specific scale while the area of significant correlation is much less than 5% (95% confidence level), the significant region is so extensive that is very unlikely for this to happen by chance. Concluding that the model fits very well with the data obtained in the case of Region IV with seasonality with the data from four Mexican states.

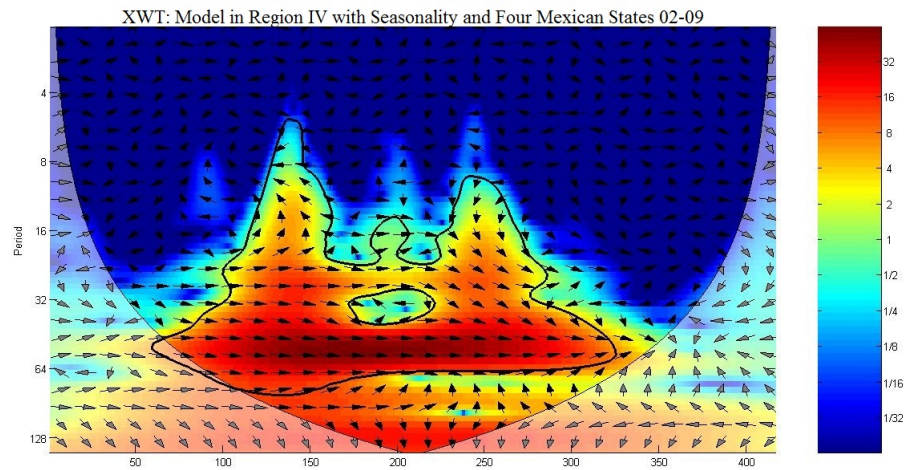


Figure 4.9: Cross Wavelet Transform of the model (1.3) Region IV with Seasonality compared with the Four States data. The relative phase relationship is shown as arrows (with in-phase pointing right, anti-phase pointing left and if the four states series leading the model pointing straight down).

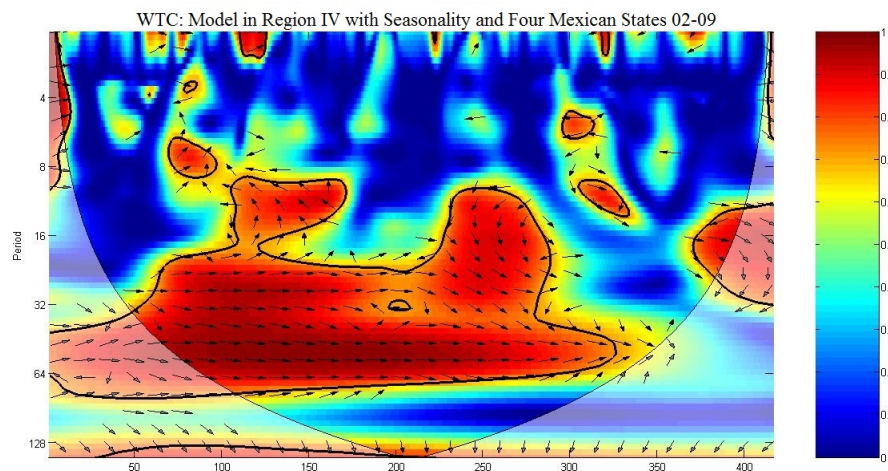


Figure 4.10: Squared Wavelet Transform Coherence. The thick contour shows the 5% significance level against red noise. We can see a significant section showing in-phase behavior.

4.4 Comparison with Cuernavaca Data

In a second experiment we have taken some solutions from the model (1.3) to compare with data from the city of Cuernavaca. Data from Cuernavaca represents the number of Dengue cases by day from 2008 to 2009. This time we selected region I of the model (see chapter 3, table (3.4)) and we forced periodicity considering that the reproduction behavior of mosquito varies periodically as the seasons in a year; this is due to the fact that mosquito spreads easier when the climate is warm and there is humidity while it spreads hardly when in cold and dry seasons. The Continuous

Wavelet Transform and time series are shown for both, the model and Cuernavaca data, in figure 4.11.

In each graph in figures 4.11A and 4.11C the cone of influence (COI) where edge effects might distort the picture is shown as a lighter shade. For both, the vertical left axis of the CWT indicates period (in days). Figure B represents the Time Series of the city of Cuernavaca showing the number of cases per day for years 2008 to 2009 proportional to the population. Figure D shows the time series for the model (1.3) with the number of cases per day proportional to the population.

The vertical right axis is the color scale used to get a better distinction between the different powers which appear in the CWT where red is higher and blue is less. The horizontal axis indicates time (in days) for both time series and CWT.

The Continuous Wavelet Transform (CWT) for the city of Cuernavaca is shown up in the figure 4.11A. There is high power at period greater than 64 between time interval of 120-400 days. The thick contour designates de 5% significance level (95% confidence level) against red noise and it is found in a band of 2-8 period at days around 150-300. Also, we observe in the time series (below) a curve that varies very quickly shaking. If we observe beyond all the little "shakes" we can distinguish one high peak near day 180 which reaches 45 infected that day, then it decreases to climb again by day 450 but reaching only till 33. Finally there is a small peak around day 585 and reaches near 10.

The CWT of the model (1.3) Region I with seasonality is displayed in figure 4.11C. We selected a section of the data to fit the size and interval length of Cuernavaca data: we have chosen from day 11300 to 11032. Comparing both CWT in figure 4.11 we notice that both share same colors (indicating the highest power) at almost same days. Both have high power at period greater than 128 from day 300-400. To confirm this we proceed to calculate the Cross Wavelet Transform (XWT) and it looks as shown in figure 4.12.

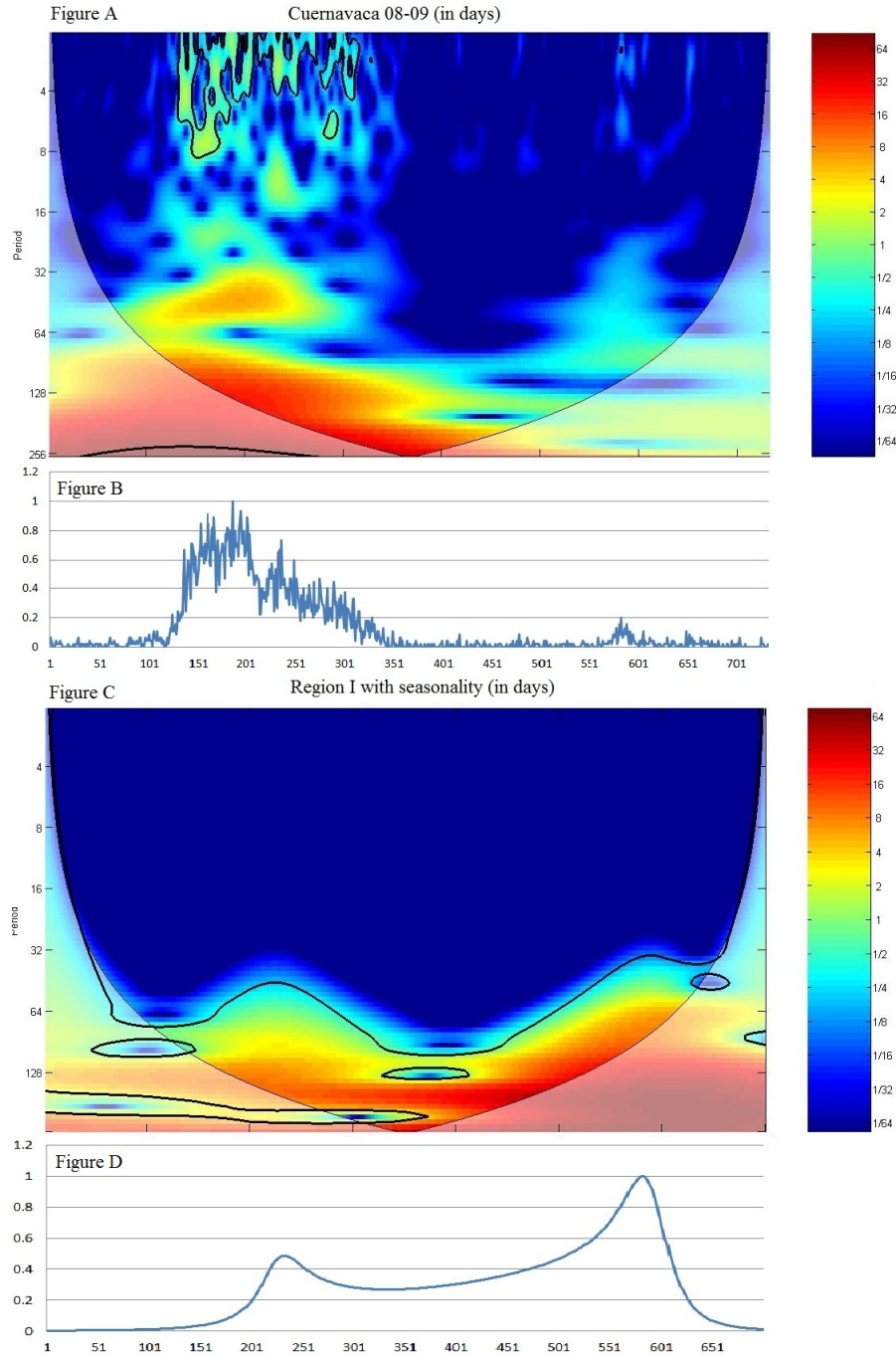


Figure 4.11: Figure A: Continuous wavelet transform of a real data basis from the city of Cuernavaca, Morelos and its time series (Figure B) below showing the number of cases per day for years 2008 to 2009. Figure C: continuous wavelet transform of the model (1.3) Region I (see chapter 3, table (3.4) with Seasonality and its time series (Figure D). Refer to the text for information on the axis.

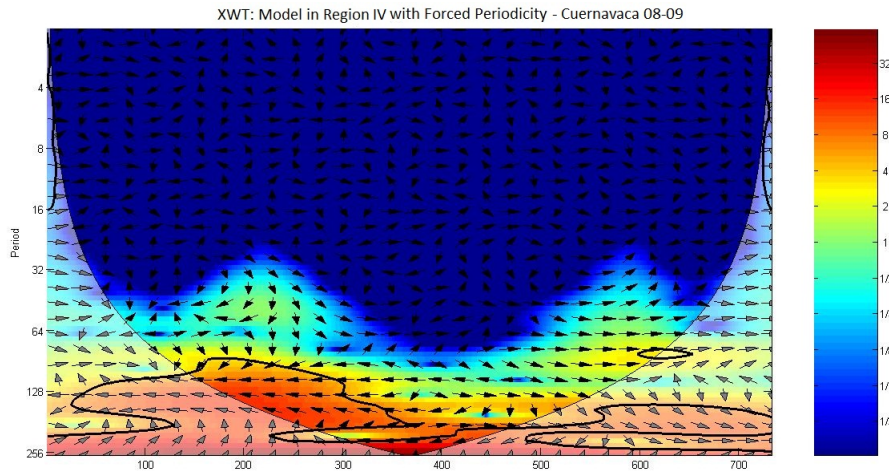


Figure 4.12: Cross Wavelet Transform of the model Region IV with Seasonality and Cuernavaca city data. The relative phase relationship is shown as arrows (with in-phase pointing right, anti-phase pointing left).

The XWT shown in figure 4.12 reveals an anti-phase behavior inside the thick contour of 5% significance level against red noise which implies significant common power in the 96-128 band from day 150-330. Nevertheless outside the contour but inside the COI we can see the arrows pointing mostly to the right where there is high power claiming the signals are in phase, but pointing at every direction at low periods with very low power.

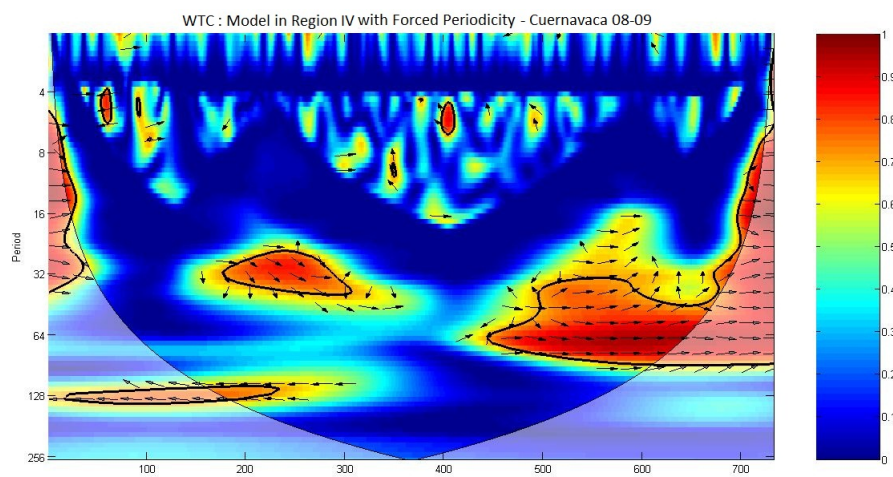


Figure 4.13: Coherence of the model Region IV with Seasonality and real data from the city of Cuernavaca.

To proceed and get more this information in this regard we continue to calculate the Coherence (WTC) for both series in order to see how coherent the XWT is in time frequency space in figure 4.13.

By looking at the red sections indicating high power in figure 4.13 we can conclude that both series share common high power at certain times and that they are coherent at this regions since the arrows inside point to the right. The biggest areas where they share common high power is at period band 24-40 around days 180-300, and also at period band from 32-64 period around days 450-600. We can notice some smaller areas between period 4-8 in between 50-500 days.

Coherence in figure 4.13 shows many significant sections inside a thick contour of 5% significance level against red noise. One of the biggest significant section is at period 24-40 band during 180-300 days. There we can see arrows are pointing down-right, but there is no in-phase or anti-phase behavior. Another big significant section, and more interesting, is at band from 32-64 period around days 450-600. There we can see in-phase behavior. This implies that there is a linear relation between both series and the model can be used to study this case.

4.5 Comparison with Google Trends Data

We also analyzed data obtained from Google Trends registered for Mexico (from January 12th 2003 to September 8th 2012) which is also organized by weeks and gave us 504 values. The time series is shown on figure 4.14B.

We can see the Continuous Wavelet Transform (CWT) for data from Google Trends on top of figure 4.14. The power is concentrated among weeks 276 to 408 and between a period of 16 to 64.

In order to compare Google Trends data with data obtained from the solution of the model (1.3), we selected data in Region IV with Seasonality. We reduced the database to have the same number of values as we got from Google Trends. More precisely, we set an interval of time with same data size than Google Trends database. We took data from day 6160 to 9681 separated by weeks. Thus, we took same number of data from the model and we kept the distance between each value that, in this case, was of one week. The CWT and time series we obtained from the model is presented at the bottom of figure 4.14.

We can compare both CWT in figure 4.14. We can see that there are similarities in the shape, although the mainly concentrated power appears at different weeks.

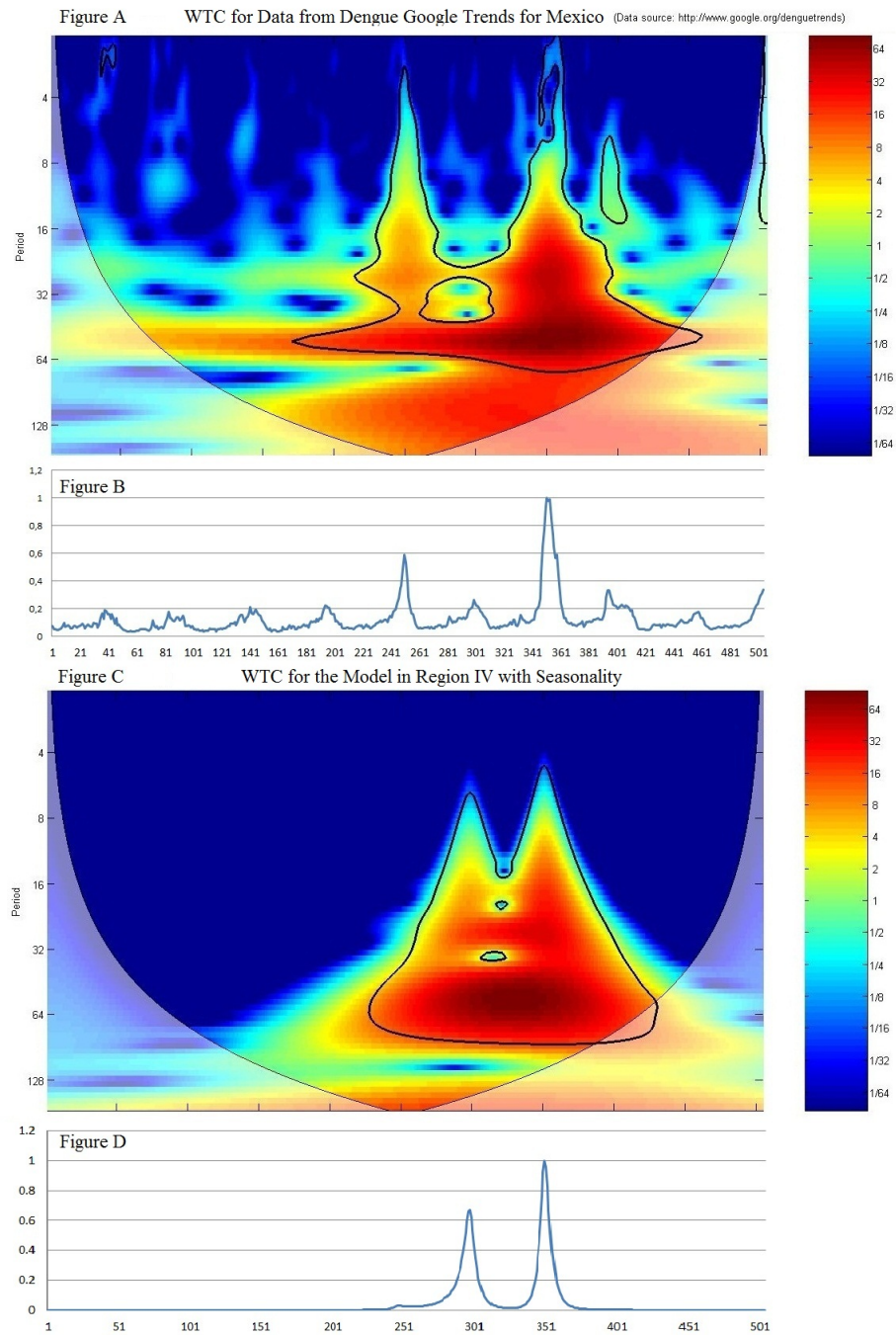


Figure 4.14: Figure A: Continuous wavelet transform of real data proportionated by Google Trends of Dengue in Mexico per week and, Figure B: its Time Series. Figure C: Continuous Wavelet Transform of data obtained using the model (1.3) in region IV with Seasonality separated by weeks and, Figure D: its Time Series.

In the top of figure 4.14, with WTC corresponding to Google data, power is shown to be stronger mainly from 32 to 64 period, although there is some small dark red that goes from 16 to 64 between weeks 330 to 380. In the bottom of figure

4.14, WTC which corresponds to the model, we have the power concentrated mainly at weeks from 250 to 400 with a remarkable moment between period 32 to 64. The other figure below has its power concentrated from weeks 280 to 400 and stays inside of the 5% significance contour.

Now we proceed to finding the XWT for both signals as shown in figure 4.15. In this graph we noted that there is a big red area indicating that there are coincidences in data obtained in Google Trends with the data from the model. The arrows pointing mostly to the right show that there is linear relation among both signals.

To confirm this conclusions we examine the Coherence between both data series using the WTC. The coherence can tell us whether the data is related, inverse related or not related at all.

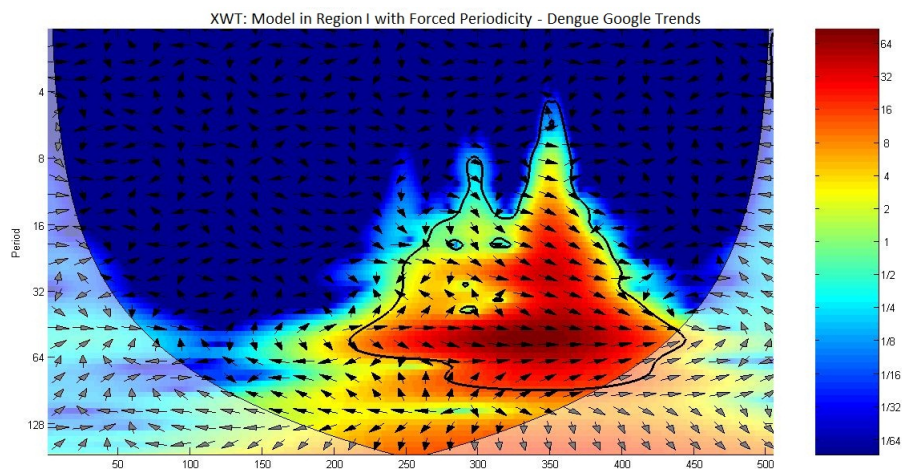


Figure 4.15: Cross Wavelet Transform of the model with forced periodicity and real data from Google Trends

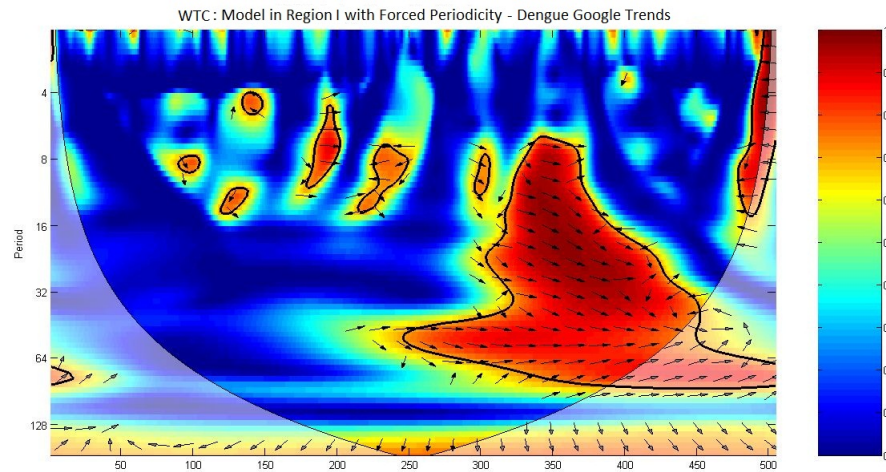


Figure 4.16: Wavelet Coherence of the model with forced periodicity and real data from Google Trends

In figure 4.16 we can see that is almost directly relate as the arrows point right from week 300 to 400 near period 64. We observe that there is a relation between data. Data has coherence. So, we can say that the model adjust also to this situation.

4.6 Conclusions

In this chapter we compared the model with three different Mexican databases taken from different regions with different sizes (a city, four states, the entire country), obtained from different sources (Mexican Dengue databases and Google Dengue Trends), with different length and interval of time. The model seems to adjust in some cases to what is shown in the real databases in each case, which make us conclude that the model is not too far from explaining reality.

Chapter 5

Conclusions

In this study we have presented a new model which describe the dynamics of dengue disease with two strains and includes a latency stage where humans are infected but are not yet infectious. Each human in the population can be infected with dengue twice at most in his lifetime before it gains immunity to the disease.

We have discussed the values of parameters and we calculated the R_0 of the disease. We distinguished that the parameters which determine the dynamics of the disease are: the force of infection human to mosquito (α_i), the force of infection mosquito to human (β_i) and the duration of the latency stage (ϕ_i). Based on that, we found regions in the parameter space such that the solutions of our system of equations show a behavior which can be compared to those observed in real situations in Mexico. The single study of the parameters and all the regions where they can have biological sense is very complicated from a mathematical point of view in the sense that the space of parameters is huge and it is not feasible to do a blind search. However, we used the information we had to place the values for some parameters between some limitations and we reduced our space of search to concentrate in the values of those parameters that can be somehow manipulated through the implementation of control strategies in a population and that we know have more.

Obviously, finding the specific values of parameters which better approximate to the know data, like the databases of Mexican states that were studied here, is a complex problem and can be better studied using optimization methods. Since this is by itself a problem which deserves special attention and dedication, and that would take us far from the objective of this study, we decided to keep it as a future project for now.

We used a computational software to find the algebraic expression for the equilibrium points but due to the complexity of the model the software failed to give us all of them. Numerically, we solve to find six of which only four were feasible. The disease-free equilibrium point, the equilibrium point were only one strain survives (one for each strain), and the equilibrium point were both strains coexist are these equilibrium points. When looking for the bifurcation point for β_i , we tried to make use of the Sotomayor Theorem, but we failed due to the complexity of the model and it is left to future studies. To solve our immediate problem, we found this bi-

furcation point for β_i only with pen and paper.

The selection of parameters in the different regions were taken due to the observed similarity they had with the real data we wanted to study. Simulations were done to determine if we could obtain some information about the behavior of the disease and helps us to clarify its dynamics. Simulations presented here show the dynamics of dengue as expected and seen in real life.

When using wavelets as a tool to verify if this model can be used to describe the dengue dynamics in a given population by comparing the solution of the model (1.3) with real data bases, we found that with the use of wavelets we can also evaluate the quality of the real data. If the database is good and large enough to contain the information of the development of dengue in a community, the model we present could adjust well as we have seen in chapter 4. Also, there are many options to select the interval of time in the solution of the model with which we would compare with real data and this influences the results of the comparison. In some cases we presented here, the model simply failed to adjust the real data.

New questions surged from this study which are left for future projects. We know that some prevention measures have been taken inside the Mexican population by the sanitary authorities in an effort to get control and reduce the damage that the disease causes among humans. These control measures must be incorporated in the model to analyze the effect they are causing in the behavior of the disease, to see, for example, if any of these measures is having a significant effect in reducing the damage in the population or if it has any effect at all. In the case of introducing vaccination in a population where the disease has been acting for years, which would be the case if inoculation is applied to the population, we could adjust the model and analyze its effect in the community.

Appendix A

Operator $\phi(K)$

Given

$$A_1 = \frac{\alpha_1 (I_1 + Y_1)}{N}$$

$$A_i = \frac{\alpha_2 (I_2 + Y_2)}{N}$$

$$B_i = \frac{\beta_1 V_1}{M}$$

$$B_i = \frac{\beta_2 V_2}{M}$$

Let $K = (A_1, A_2, B_1, B_2)'$ then we substitute the expressions given in the model (2.14) into the definitions of A_i and B_i to obtain a new system of four equations in terms of A_i and B_i . We obtain the system $K = \phi(K)$, that is

$$\phi(K) = \begin{pmatrix} K_1 \\ K_2 \\ K_3 \\ K_4 \end{pmatrix} \quad (\text{A.1})$$

where

$$\begin{aligned} K_1 &= \frac{\alpha_1 \phi_1 B_1 \left(\frac{1}{(\phi_1 + \mu)(\gamma_1 + \mu)} + \frac{\sigma_1 \eta_2 \gamma_2 \phi_2 B_2}{(\phi_2 + \mu)(\gamma_2 + \mu)(\eta_2 + \mu)(\sigma_1 B_1 + \mu)(\phi_1 + \mu)(\gamma_1 + \mu + m_1)} \right)}{\kappa_1} \\ K_2 &= \frac{\alpha_2 \phi_2 B_2 \left(\frac{1}{(\phi_2 + \mu)(\gamma_2 + \mu)} + \frac{\sigma_2 \eta_1 \gamma_1 \phi_1 B_1}{(\phi_1 + \mu)(\gamma_1 + \mu)(\eta_1 + \mu)(\sigma_2 B_2 + \mu)(\phi_2 + \mu)(\gamma_2 + \mu + m_2)} \right)}{\kappa_2} \\ K_3 &= \frac{\beta_1 A_1}{\delta + A_1 + A_2} \\ K_4 &= \frac{\beta_2 A_2}{\delta + A_1 + A_2} \end{aligned} \quad (\text{A.2})$$

where

$$\begin{aligned}
\kappa_1 &= 1 + \frac{B_1}{\phi_1 + \mu} + \frac{B_2}{\phi_2 + \mu} + \frac{B_1 \phi_1}{(\phi_1 + \mu)(\gamma_1 + \mu)} + \frac{B_2 \phi_2}{(\phi_2 + \mu)(\gamma_2 + \mu)} + \frac{B_1 \phi_1 \gamma_1}{(\phi_1 + \mu)(\gamma_1 + \mu)(\eta_1 + \mu)} \\
&+ \frac{B_2 \phi_2 \gamma_2}{(\phi_2 + \mu)(\gamma_2 + \mu)(\eta_2 + \mu)} + \frac{B_1 \phi_1 \gamma_1 \eta_1}{(\phi_1 + \mu)(\gamma_1 + \mu)(\eta_1 + \mu)(\sigma_2 B_2 + \mu)} + \frac{B_2 \phi_2 \gamma_2 \eta_2}{(\phi_2 + \mu)(\gamma_2 + \mu)(\eta_2 + \mu)(\sigma_1 B_1 + \mu)} \\
&+ \frac{B_1 \sigma_1 B_2 \phi_2 \gamma_2 \eta_2}{(\phi_2 + \mu)(\gamma_2 + \mu)(\eta_2 + \mu)(\sigma_1 B_1 + \mu)(\phi_1 + \mu)} + \frac{B_2 \sigma_2 B_1 \phi_1 \gamma_1 \eta_1}{(\phi_1 + \mu)(\gamma_1 + \mu)(\eta_1 + \mu)(\sigma_2 B_2 + \mu)(\phi_2 + \mu)} \\
&+ \frac{\phi_1 B_1 \sigma_1 B_2 \phi_2 \gamma_2 \eta_2}{(\phi_2 + \mu)(\gamma_2 + \mu)(\eta_2 + \mu)(\sigma_1 B_1 + \mu)(\phi_1 + \mu)(\gamma_1 + \mu + m_1)} \\
&+ \frac{\phi_2 B_2 \sigma_2 B_1 \phi_1 \gamma_1 \eta_1}{(\phi_1 + \mu)(\gamma_1 + \mu)(\eta_1 + \mu)(\sigma_2 B_2 + \mu)(\phi_2 + \mu)(\gamma_2 - \mu + m_2)} \\
&+ \frac{\gamma_1 \phi_1 \phi_1 B_1 \sigma_1 B_2 \phi_2 \gamma_2 \eta_2}{\mu(\phi_2 + \mu)(\gamma_2 + \mu)(\eta_2 + \mu)(\sigma_1 B_1 + \mu)(\phi_1 + \mu)(\gamma_1 + \mu + m_1)} \\
&+ \frac{\gamma_2 \phi_2 B_2 \sigma_2 B_1 \phi_1 \gamma_1 \eta_1}{\mu(\phi_1 + \mu)(\gamma_1 + \mu)(\eta_1 + \mu)(\sigma_2 B_2 + \mu)(\phi_2 + \mu)(\gamma_2 - \mu + m_2)} \\
\kappa_2 &= 1 + \frac{B_2}{\phi_2 + \mu} + \frac{B_1}{\phi_1 + \mu} + \frac{B_2 \phi_2}{(\phi_2 + \mu)(\gamma_2 + \mu)} + \frac{B_1 \phi_1}{(\phi_1 + \mu)(\gamma_1 + \mu)} + \frac{B_2 \phi_2 \gamma_2}{(\phi_2 + \mu)(\gamma_2 + \mu)(\eta_2 + \mu)} \\
&+ \frac{B_1 \phi_1 \gamma_1}{(\phi_1 + \mu)(\gamma_1 + \mu)(\eta_1 + \mu)} + \frac{B_2 \phi_2 \gamma_2 \eta_2}{(\phi_2 + \mu)(\gamma_2 + \mu)(\eta_2 + \mu)(\sigma_1 B_1 + \mu)} + \frac{B_1 \phi_1 \gamma_1 \eta_1}{(\phi_1 + \mu)(\gamma_1 + \mu)(\eta_1 + \mu)(\sigma_2 B_2 + \mu)} \\
&+ \frac{B_2 \sigma_2 B_1 \phi_1 \gamma_1 \eta_1}{(\phi_1 + \mu)(\gamma_1 + \mu)(\eta_1 + \mu)(\sigma_2 B_2 + \mu)(\phi_2 + \mu)} + \frac{B_1 \sigma_1 B_2 \phi_2 \gamma_2 \eta_2}{(\phi_2 + \mu)(\gamma_2 + \mu)(\eta_2 + \mu)(\sigma_1 B_1 + \mu)(\phi_1 + \mu)} \\
&+ \frac{\phi_2 B_2 \sigma_2 B_1 \phi_1 \gamma_1 \eta_1}{(\phi_1 + \mu)(\gamma_1 + \mu)(\eta_1 + \mu)(\sigma_2 B_2 + \mu)(\phi_2 + \mu)(\gamma_2 + \mu + m_2)} \\
&+ \frac{\phi_1 B_1 \sigma_1 B_2 \phi_2 \gamma_2 \eta_2}{(\phi_2 + \mu)(\gamma_2 + \mu)(\eta_2 + \mu)(\sigma_1 B_1 + \mu)(\phi_1 + \mu)(\gamma_1 - \mu + m_1)} \\
&+ \frac{\gamma_2 \phi_2 \phi_2 B_2 \sigma_2 B_1 \phi_1 \gamma_1 \eta_1}{\mu(\phi_1 + \mu)(\gamma_1 + \mu)(\eta_1 + \mu)(\sigma_2 B_2 + \mu)(\phi_2 + \mu)(\gamma_2 + \mu + m_2)} \\
&+ \frac{\gamma_1 \phi_1 B_1 \sigma_1 B_2 \phi_2 \gamma_2 \eta_2}{\mu(\phi_2 + \mu)(\gamma_2 + \mu)(\eta_2 + \mu)(\sigma_1 B_1 + \mu)(\phi_1 + \mu)(\gamma_1 - \mu + m_1)}
\end{aligned}$$

(A.3)

Bibliography

- [1] Addison Paul S. Wavelet Transforms and the ECG: a Review. Institute of Physics Publishing: Physiological Measurement 26 (2005) R155-R199.
- [2] Anderson R.M., May R.M. Infectious Diseases of Humans. Oxford Science Publications. Great Britain.
- [3] Bourdet Dominique, Ayoub J.A. and Pirard Y.M. Use of pressure derivative in Well-Test interpretation. SPE Formation Evaluation, June 1989.
- [4] Brauer, Fred. (2008) Compartmental Models in Epidemiology. Mathematical Epidemiology. Springer.
- [5] Cazelles Bernard, Chavez Mario, McMichael Anthony J., Hales Simon. Nonstationary Influence of El Niño on the Synchronous Dengue Epidemics in Thailand. PLOS Medicien. Volume 2, Issue 4 e106. April 2005.
- [6] Cazelles Bernard, Chavez Mario, Constantin de Magny Guillaume, Guégan Jean-Francois and Hales Simon. Time-dependent Spectral Analysis of Epidemiological Time-series with Wavelets. Journal of The Royal Society Interface 2007, 4, 625-626.
- [7] Chowell G., Hengartner N.W., Castillo-Chavez C., Fenimore P.W., Hyman J. M.. The Basic Reproductive Number of Ebola and the effects of Public Health Measures: The Cases of Congo and Uganda.
- [8] Cooper G.R.J., Cowan D.R. Comparing Time Series using Wavelet-based Semblance Analysis. Computers Geosciences 34 (2008) 95-102.
- [9] Daubechies Ingrid. Ten Lectures on Wavelets. CBMS-NSF Regional Conference Series in Applied Mathematics. SIAM 1992.
- [10] Derouich M., Boutayeb A., Twizell E.H. A Model of Dengue Fever. BioMedical Engineering Online. Open Access 2003.
- [11] Diekmann O., Heesterbeek J.A.P. and Metz J.A.J. On the Definition and the Computation of the Basic Reproduction Ratio R_0 in Models for Infectious Diseases in Heterogeneous Populations. Journal of Mathematical Biology Springer-Verlag 1990.
- [12] Diekmann O., Heesterbeek J.A.P. Mathematical epidemiology of infectious diseases: model building, analysis and interpretation. Wiley Series in Mathematical and Computational Biology. 2000.

- [13] Diekmann O., Heesterbeek J.A.P. and Roberts M. G. The Construction of Next-Generation Matrices for Compartmental Epidemic Models. *Journal of the Royal Society Interface* 7 (2010) 873-885.
- [14] Esteva Lourdes, Gómez Guillermo, Hernández Juan, Zepeda Marco. *Matemáticas y Epidemiología*. Grupo de Bio-Matemáticas, Depto. de Matemáticas, Facultad de Ciencias, UNAM. Ciencias No. 24 Octubre 1991.
- [15] Farge Marie. Wavelet transforms and their applications to turbulence. *Annu. Rev. Fluid Mech.*, 24, 395-457. 1992.
- [16] Favier Charly, Degallier Nicolas, Dubois Mar A. Dengue Epidemic Modelling: Stakes and Pitfalls. APBN Vol. 9 No. 22, 2005.
- [17] Feng, Zhilan and Velasco-Hernández, Jorge X. Competitive Exclusion in a Vector-host Model for the Dengue Fever. *Journal of Mathematical Biology* (1997) 35, 523-544.
- [18] Ferreira Claudia P., Pinho Suani T.R., Esteva Lourdes, Barreto F.R., Morato e Silva V.C., Teixeira M.G.L. Modelling of Dynamics of Dengue Real Epidemics. *Anais do CNMAC*.
- [19] Fischer Wayne. Using the CWT to Characterize Differences between Signals from Non-Cleated and Cleated Turf Shoes.
- [20] Graps Amara. An introduction to Wavelets. Institute of Electrical and Electronics Engineers, Inc. 1995.
- [21] Grinsted A., Moore J. C., and Jevrejeva S.. Application of the Cross Wavelet Transform and Wavelet Coherence to Geophysical Time Series. *Nonlinear Processes in Geophysics* (2004) 11, 561-566.
- [22] Guardiola John, Vecchio Antonia. The Basic Reproduction Number for Infectious Dynamics Models and the Global Stability of Stationary Points. November 26, 2003.
- [23] Harrington, L. C., Scott, T. W., Lerdthusnee, K., et al. (2005) Dispersal of the dengue vector *Aedes aegypti* within and between rural communities. *American Journal of Tropical Medicine and Hygiene*, 72, 209-220.
- [24] Heffernan, J. M., Smith, R.J. and Wahl L.M. Perspectives on the Basic Reproductive Ratio. *Journal of the Royal Society Interface*. 2, 281-293, June 7, 2005.
- [25] Holland Jones James. Notes on R_0 . Department of Anthropological Sciences, Stanford University. May 1, 2007.
- [26] Hsieh Ying-Hen and Ma Stefan. Intervention Measures, Turning Point, and Reproduction Number for Dengue, Singapore, 2005. *The American Society of Tropical Medicine and Hygiene* 80(1), 2009.

- [27] Hurford Amy, Cownden, Day Troy. Next-Generation Tools for Evolutionary Invasion Analyses. *Journal of the Royal Society Interface* 2009.
- [28] Johansson Michael A., Cummings Derek A. T., Glass Gregory E.. Multiyear Climate Variability and Dengue - El Niño Southern Oscillation, Weather, and Dengue Incidence in Puerto Rico, Mexico and Thailand: A Longitudinal Data Analysis. *PLOS Medicine*, November 2009, Volume 6, Issue 11.
- [29] Kermack W. O., McKendrick A. G. A Contribution to the Mathematical Theory of Epidemics. *Proceedings of the Royal Society of London. Series A, Containing Papers of a Mathematical and Physical Character*, volume 115, Issue 772 (August 1, 1927), 700-721. JSTOR.
- [30] Lajmanovich Ana and Yorke James A. A Deterministic Model for Gonorrhoea in a Nonhomogeneous Population. *Mathematical Biosciences* 28, 221-236 (1976)
- [31] Lipsitch Marc, Mills Christina, Robins James. Estimates of the Basic Reproductive Number for 1918 Pandemic Influenza in the United States.
- [32] Mantilla P. Ignacio, Ruíz V. Jorge Mauricio. Un Método Numérico para el Cálculo de la Velocidad de Propagación de una Epidemia. *Boletín de Matemáticas, Nueva Serie, Volumen IV* (1997), pp 115-116.
- [33] Maraun D. and Kurths J.: Cross Wavelet Analysis. Significance Testing and Pitfalls, *Nonlin. Proc. Geoph.* 11(4), 505-514, 2004.
- [34] Maraun D., Kurths J. and Holschneider M.: Nonstationary Gaussian Processes in Wavelet Domain: Synthesis, Estimation and Significance Testing. *Phys. Rev. E* 75, 016707, 2007.
- [35] Montesinos-López Osval Antonio, Hernández-Suárez Carlos Moisés. Modelos Matemáticos para Enfermedades Infecciosas. *Salud Pública de México* vol. 49, no.3, mayo-junio de 2007.
- [36] Mosquera Luis A., Perea Milton H. Modelo Matemático para la Enfermedad del Dengue. *Boletín de Matemáticas, Nueva Serie, Volumen XIII No. 2* p. 176-185, 2006.
- [37] Mukandavire Zindoga, Liao Shu, Wang Jin, Gaff Holly, Smith David L. and Morris J. Glenn, Jr. Estimating the Reproductive Numbers for the 2008-2009 Cholera Outbreaks in Zimbabwe. *PNAS* May 24, 2011, vol. 108, no. 21.
- [38] Mukhopadhyay B., Bhattacharyya B.. Diffusion Induced Shift of Bifurcation Point in a Mangrove Ecosystem Food-chain Model with Harvesting.
- [39] Nagao Yoshiro and Koelle Katia. Decreases in Dengue Transmission may act to Increase the Incidence of Dengue Hemorrhagic Fever. *PNAS* February 12, 2008, vol. 105, no. 6.
- [40] Nyabadza Farai. Modelling the Role of Prophylaxis in Malaria Prevention. *International Journal and Life Sciences* 4:1 2008.

- [41] Osinga H.M., Hogan S.J., Champneys A.R., Krauskopf B., di Bernardo M., Wilson R.E., and Homer M.E. *Nonlinear Dynamics and Chaos*. EMAT 33100. Institute of Physics Publishing, 2002.
- [42] Pérez-Peraza J., Velasco V. and Kavлакov S. Wavelet Coherence Analysis of Atlantic Hurricanes and Cosmic Rays. *Geofísica Internacional* 47(3), 231-244 (2008).
- [43] Polikar Robi. Rowan University, College of Engineering Web Server: The Wavelet Tutorial Online. 1999. <http://users.rowan.edu/polikar/WAVELETS/WTtutorial.html>
- [44] Prasad Vadrevu Krishna, Choi Yonghoon. Wavelet Analysis of Airborne CO_2 Measurements and Related Meteorological Parameters over Heterogeneous Landscapes. *Elsevier Journal, Atmospheric Research* 102 (2011) 77-90.
- [45] Smith David L., McKenzie F. Ellis, Snow Robert W., Hay Simon I. Revisiting the Basic Reproductive Number for Malaria and its Implications for Malaria Control. 2007.
- [46] Reiner Robert C. Jr., King Aaron A., Emch Michael, Yunus Mohammad, A. S. G. Faruque and Mercedes Pascual. Highly Localized Sensitivity to Climate Forcing Drives Endemic Cholera in a Megacity. *PNAS* February 7, 2012, Vol. 109, no. 6.
- [47] Torrence Christopher and Compo Gilbert P. *A Practical Guide to Wavelet Analysis*. Bulletin of the American Meteorological Society (1998).
- [48] van den Driessche P., Watmough James. Reproduction Numbers and Sub-threshold Endemic Equilibria for Compartmental Models of Disease Transmission. *Mathematical Biosciences* 180 (2002) 29-48, Elsevier.
- [49] Watmough James. Computation of the Basic Reproduction Number. MITACS-PIMS Summer School on Mathematical Modelling of Infectious Disease, University of Alberta. May, 2008.
- [50] Velasco-Hernández Jorge X. Noviembre 11, 2009.
- [51] Population Dynamics of Dengue: Patterns of Immunity Revisited.
- [52] "Fuente de los datos: Evolución del dengue en Google (<http://www.google.org/denguetrends>)".
- [53] Wikipedia (http://en.wikipedia.org/wiki/Dengue_fever).
- [54] Software XPPAUT <http://www.math.pitt.edu/bard/xpp/xpp.html>.
- [55] Ge Z. Significance Tests for the Wavelet Power and the Wavelet Power Spectrum. *Annales Geophysicae* 25, 2259-2269, 2007.